Recent advances in ultrasonography (US) technology, including harmonic imaging and the availability of US contrast agents, have improved the usefulness of US contrast agents in the characterization of focal liver lesions, including HCC.[17–21] To our knowledge, this is the first study correlating parametric imaging using contrast enhanced ultrasonography (CEUS) and SonoVue (Bracco, Milan, Italy), a second generation ultrasound contrast agent, with the degree of cellular differentiation.

The aim of this study is, by evaluating quantitatively the blood flow parameters, such as the β-value and A value, and further utilizing parametric imaging which visualizes these parameters, to determine whether the blood parameters and parametric imaging correlate with the degree of cellular differentiation.

METHODS

Patients

THE STUDY SUBJECTS were 49 patients with 49 HCCs ranging from 10 to 55 mm (mean ± SD, 27.2 ± 12.2 mm) that had been visualized clearly on conventional sonograms for the first time during the 12 months from July 2005 through to June 2006. The patients included 29 men and 20 women, with an age range of 43–82 years (mean age, 65.3 ± 10.0). For patients with more than one focal lesion, we selected the largest for this study. Signed informed consent was obtained from all patients in accordance with the rules of the ethics committee at Tokyo Medical University. Specimens from hepatic masses were obtained with a 20-gauge US-guided FNB. The degree of cellular differentiation (defined as well [w], moderately [m] or poorly [p] differentiated HCC) was determined according to the International Working Party classification.[22]

Imaging techniques

SonoVue was injected as 1.5 mL bolus into an antecubital vein using a 21-gauge peripheral intravenous cannula, followed by an injection of 10 mL saline solution at a rate of 1.0 mL/s. The ultrasound equipment used was SSA-770 A (Aplio; Toshiba Medical Systems, Otawara, Japan) with a 3.75 MHz convex transducer (PSK-375BT). The imaging mode was wideband harmonic imaging (commercially named as Pulse subtraction) with transmission and reception frequencies of 3.75 and 7.5 MHz, respectively. When the suspected lesion was identified, a dynamic CEUS was performed with the focus depth beyond the area of interest, using the following settings: frame rate, 15 frame per seconds (fps); gain, 80–82; dynamic range, 35 dB. A low mechanical index (MI) (0.07–0.08) was selected to avoid the disruption of microbubbles.

The enhancement patterns of the HCC were studied during the vascular phases up to 3.0 min, including the arterial (0–49 s), portal (50–89 s) and the late (90–180 s) phases. Images and clips were stored on hard disk for offline analysis.

Imaging analysis

Quantitative parametric analysis

The exact time course of the protocol is shown in Figure 1. Prototype software dedicated to the SSA-770 A was used to calculate time intensity curves (TIC) for the HCC. Regions of interest (ROI) were set corresponding to the whole mass. The quantification procedure was processed for each pixel of the selected region on the frame sequence during the selected period, that is the arterial phase (from 0 to 49 s after injection), with position correction. Time intensity curves were composed with the theoretical curve SI(t) obtained with the following formula:[23]

$$SI(t) = A(1 - e^{-\beta}) \quad (1)$$

After this procedure, parametric curves were obtained, with which we could determine A_{peak} (A value at maximum enhancement), A_{120} (A value corresponding to time for 120 s), and β parameter value (corresponding to the exponential factor).

Results are presented as mean ± SD. A Kruskal–Wallis test was performed to compare each parametric value of the whole lesion of HCC. A *P*-value less than 0.05 was considered as statistically significant. Data were analyzed using StatMate III for Windows (Atoms, Takehara City, Japan).

Parametric imaging

Prototype PC software dedicated to the images obtained by our ultrasound system was developed for this study. The software reads the Audio Video Interleaving (AVI) image obtained by the US system, calculates the enhanced intensity on the image frame by frame, estimates the T_A value according to the TIC and reconstructs the color coded parametric image for the β-value. The β-value is defined as $1/T_A$.[23] and therefore is inversely correlated with T_A. In this study we treated the two parameters as if they meant the same.

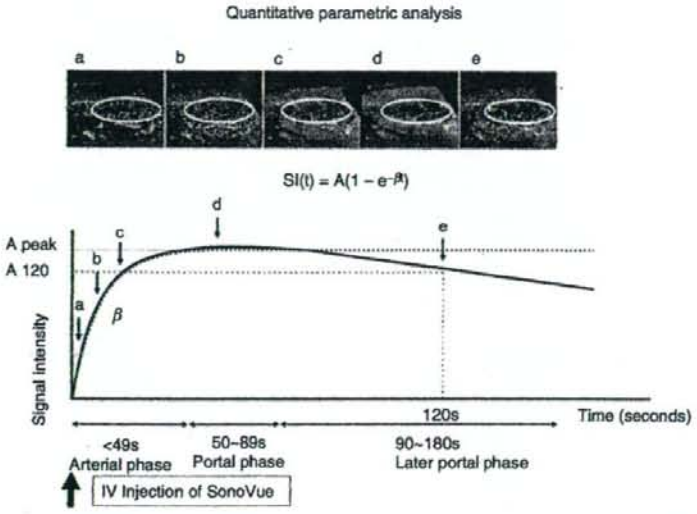

Figure 1 Bolus injection of the contrast agent formed a time intensity curve (solid line) showing that the signal intensity temporarily increased, plateaued and gradually decreased. It was possible to draw an approximate curve according to the following formula: SI $(t) = A\ (1 - e^{-\beta t})$ (dotted line). The β-value and peak of the A value were calculated from this approximate curve. In addition, A_{120} for the signal intensity 120 s later was directly calculated.

After 1.5 mL of SonoVue was injected intravenously and staining of the tumors and parenchyma was confirmed (30–40 s), microbubbles in the scanned volume were destroyed using high MI scanning under a breathhold to avoid strong motion of the lesions. The color-coded β images were displayed at the phase after reperfusion. The images at the phase when the staining reached a plateau (90–180 s) were employed for A images, reflecting A values.

Tumors were classified into three grades by one blinded reviewer according to the β images, that is, hyper β, iso β and hypo β, when the β-value in the tumor was either higher than, the same as, or lower than that in the adjacent normal liver parenchyma, respectively. Similarly, tumors were classified into three grades by one blinded reviewer according to the A images, that is, hyper A, iso A and hypo A, when the A value of the tumor was higher than, the same as, or lower than that in the adjacent normal liver parenchyma, respectively. If a tumor consisted of mixed grades, the grade with the largest area was taken to be representative. In the image analysis, tumors that were spatially and temporally homogenous and/or regular in β-value, or which showed almost the same pattern as that in the adjacent normal liver parenchyma in the β-value were classified by one blinded reviewer as homogenous β, while tumors that were heterogeneous and/or irregular color-coded by the β-value were classified as heterogeneous β. These images were correlated with the histological grades of differentiation. The Kruskal–Wallis test was used to obtain the relationship between the parametric images and the histological grades of differentiation. A *P*-value less than 0.05 was considered as statistically significant. Data were analyzed using StatMate III for Windows (Atoms, Takehara City, Japan).

RESULTS

THE FINAL DIAGNOSES of the HCCs were: w-HCC in 19 cases (38.8%), ranging in diameter from 10 to 32 mm (mean ± SD, 25.7 ± 6.9 mm); m-HCC in 22 (44.9%), ranging in diameter from 19 to 50 mm (mean ± SD, 27.8 ± 8.0 mm); and p-HCC in eight (16.3%), ranging in diameter from 22 to 55 mm (mean ± SD, 31.9 ± 11.2 mm). There was the tendency, although not significant, for more poorly differentiated tumors to have a larger diameter.

Quantitative parametric analysis

The values of the parameters extracted from the various imaging techniques are shown in Table 1. The β-value was significantly higher ($P < 0.05$) in m-HCCs than w-HCCs, whereas no significant differences were found in this parameter between the other combinations. A_{peak} value was significantly higher in m-HCC than in the other HCCs ($P < 0.001$), whereas no significant difference was found between w-HCCs and p-HCCs. The A_{120} value was significantly lower in p-HCC than in the other

Table 1 Determined mean value ± SD of β, A peak, A 120 and A ratio for the HCCs

Histological differentiation	β (s-1)	A peak (dB)	A 120 (dB)	A ratio (A peak/A 120)
w-HCCs	0.13 ± 0.04	1433.75 ± 445.66	124.50 ± 93.99	12.45 ± 4.25
m-HCCs	0.17 ± 0.05	3310.00 ± 637.35	86.95 ± 41.81	42.50 ± 3.22
p-HCCs	0.15 ± 0.07	1620.00 ± 813.63	31.20 ± 5.85	52.27 ± 25.18

β-value was significantly higher ($P < 0.05$) in moderately differentiated HCCs (m-HCCs) than well-differentiated HCCs (w-HCCs). A peak value was significantly higher in m-HCCs than in other HCCs ($P < 0.001$). An 120 value was significantly lower in poorly differentiated HCCs (p-HCCs) than in other HCCs ($P < 0.05$ for w-HCC; $P < 0.001$ for m-HCC). A value ratio (A peak/A 120) was significantly lower in w-HCCs than in another HCCs ($P < 0.001$ for m-HCC; $P < 0.01$ for p-HCC).

HCCs ($P < 0.05$ for w-HCC; $P < 0.001$ for m-HCC), while no significant difference was found between w-HCC and m-HCC. On the other hand, the A value ratio (A_{peak}/A_{120}) was significantly lower in w-HCC than in the other HCCs ($P < 0.001$ for m-HCC; $P < 0.01$ for p-HCC), whereas no significant difference was found between m-HCC and p-HCC.

Parametric imaging

The results of the association between β images and cellular differentiation are presented in Table 2. Analysis of T_A images indicated that β-values in m-HCC were higher than in the adjacent non-tumor parenchyma in all 22 samples, and were significantly higher than in the other HCCs ($P < 0.001$ for w-HCC; $P < 0.05$ for p-HCC) (Figs 2a,3a,4a). Table 3 shows that β-values in p-HCC had significantly greater variations in terms of time and space than in the other HCCs ($P < 0.001$ for w-HCC; $P < 0.01$ for m-HCC) (Fig. 4a). The results of the association between A images and the degree of differentiation are presented in Table 4. Analysis of A images indicated that the A values in w-HCC were significantly higher than those in m-HCC and p-HCC ($P < 0.001$) (Figs 2b,3b,4b).

Table 2 Parameter β of HCCs according to tumor differentiation

Histological differentiation	Hyper β	Iso β	Hypo β	Total
w-HCCs	5	8	6	19
m-HCCs	22	0	0	22
p-HCCs	4	0	4	8
Total	31	8	10	49

β-values in moderately differentiated HCCs (m-HCCs) were significantly higher than those in other HCCs ($P < 0.001$ for well-differentiated HCC [w-HCC]; $P < 0.05$ for poorly differentiated HCC [p-HCC]). Hyper β, β-value that is higher than those in the adjacent non-tumor parenchyma; Hypo β, β-value that is lower than those in the adjacent non-tumor parenchyma; Iso β, β-value that is equal to the adjacent non-tumor parenchyma.

DISCUSSION

MICROBUBBLE-BASED US contrast agents increase the intensity of the blood flow signal, improving the detection of flow in the hepatic artery and small vessels, and are as effective as CT in assessing lesion perfusion.[17] Contrast-specific modes such as advanced dynamic flow (ADF; Toshiba Medical Systems, Otawara, Japan) associated with contrast agent Levovist (Schering, Berlin, Germany) allow the evaluation of microvascularization of focal liver lesions, improving their characterization.[24] However, because Levovist's microbubbles are too sensitive to the ultrasound pulse, the intermittent scanning (i.e. non-real time imaging) method has to be used.[17] The new contrast agents, such as SonoVue, are more stable and resistant to ultrasound exposure; they radiate sufficient harmonic signals by low MI transmission power to allow continuous real time imaging.[25] Also, from the clinical point of view, real time examination with SonoVue can acquire detailed information and also is time-efficient for the examination itself. It is suggested to be superior to Levovist in the evaluation of the hemodynamic status of focal liver lesions.

Several authors have reported on the behavior of the microbubbles in HCC.[17,18,20,21,25] Solbital *et al.*[25] described a diffuse enhancement during the arterial phase that decreases during the portal venous and late phases, presenting a hypoechoic appearance in 54 out of 61 HCCs (88.5%), while in the remaining seven they found an unhomogeneous enhancement related to necrotic changes. Nicolau *et al.*[26] reported that almost all HCCs (96.2%) showed intratumoral enhancement in the arterial phase with a wash-out in the late phase in 74

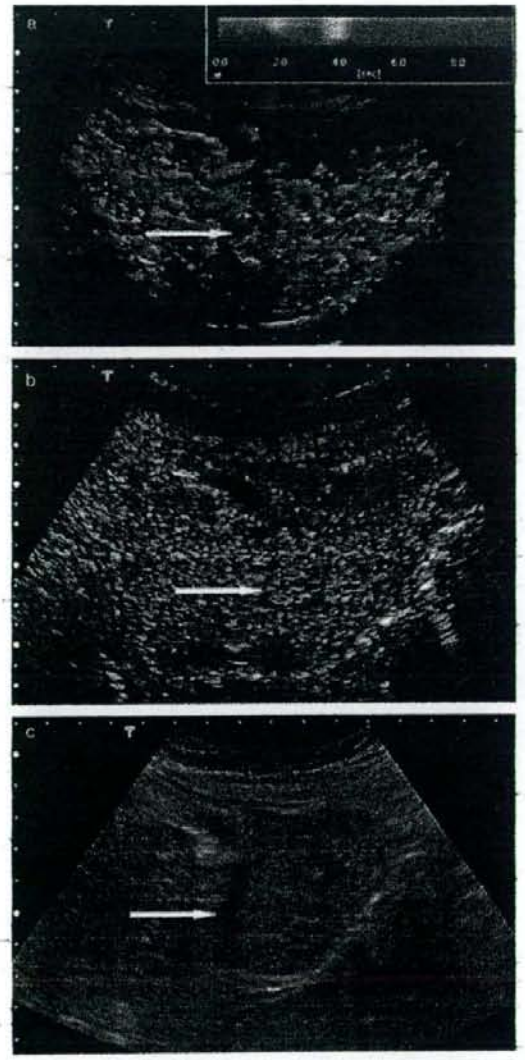

Figure 2 A 68-year-old woman with a 20 mm diameter well-differentiated hepatocellular carcinoma in the right anterior segment of her liver. (a) Arrival time (T_A) image indicates that the β-value in this tumor (arrow) is almost the same as that in the surrounding normal liver parenchyma. The distribution of β-values in this tumor shows almost the same pattern as that in the surrounding normal liver parenchyma. (b) An image obtained 140 s after contrast medium injection indicates that the A value in this tumor (arrow) is equal to that of the adjacent non-tumor parenchyma. (c) Baseline ultrasonography image shows a focal hypoechoic tumor (arrow) in the right anterior segment of the liver.

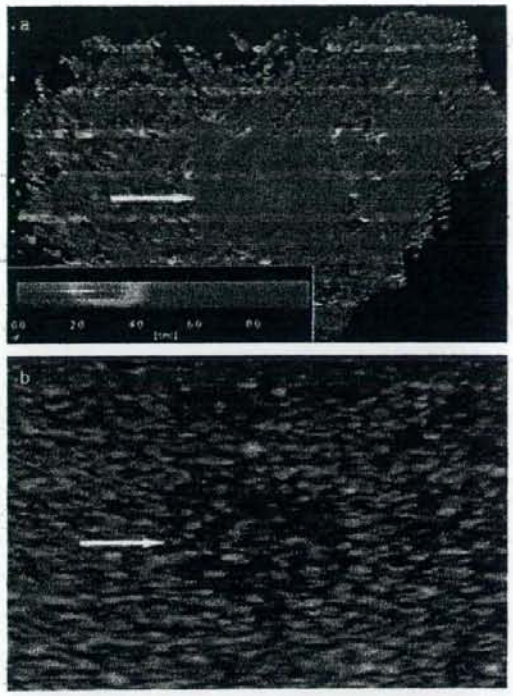

Figure 3 A 65-year-old man with a 20 mm diameter moderately differentiated hepatocellular carcinoma in the right anterior segment of his liver. (a) Arrival time (T_A) image indicates that the β-value in this tumor is higher than that of the adjacent non-tumor parenchyma. It shows blood flow coming from the marginal area to the central area in one still image. The distribution of β-values in this tumor is regular compared with the poorly differentiated hepatocellular carcinoma. (b) An image obtained 163 s after contrast medium injection indicates that the A value in this tumor (arrows) is lower than that of adjacent non-tumor parenchyma.

of 104 HCCs (71.2%). Four HCCs in their study without arterial enhancement in CEUS were found to be w-HCC. They also found significant differences between the degree of cellular differentiation in the enhancement pattern of the HCC in the portal and late phases. Fan *et al.* reported that m- to p-HCCs had significantly shorter wash-out times compared to w-HCC, suggesting that the CEUS is useful for diagnosis of the degree of differentiation of HCC.[27]

All of these studies have examined HCC continuously in real time at low acoustic transmission power with SonoVue. Although the robustness of the CEUS is

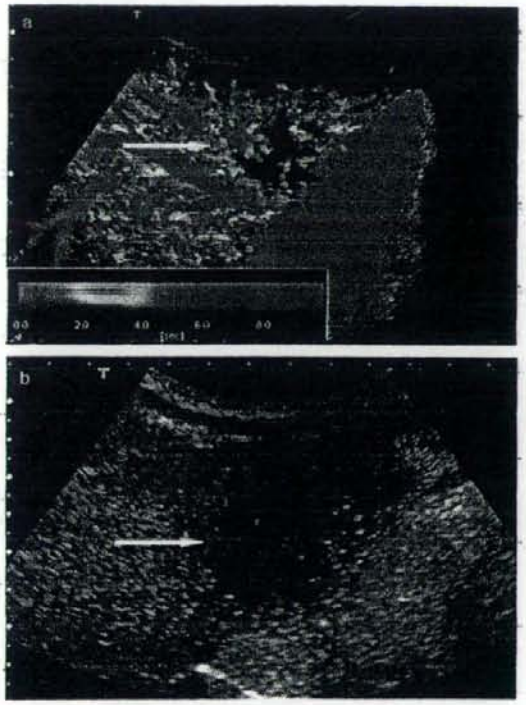

Figure 4 A 53-year-old woman with a 38 mm diameter poorly differentiated hepatocellular carcinoma in the left lobe of her liver. (a) Arrival time (T_A) image indicates that the β-value in this tumor is lower than that of the adjacent non-tumor parenchyma. The distribution of β-values in this tumor is highly heterogeneous and irregular compared with the other hepatocellular carcinomas. (b) An image obtained 136 s after contrast medium injection indicates that the A value in this tumor is significantly lower than that of the adjacent non-tumor parenchyma.

sometimes considered to be inferior to CT or MRI contrast, CEUS has an advantage over both in terms of real time image acquisition.[28] To overcome this disadvantage, we conducted this study that quantitatively evaluated the blood flow parameters such as β or A values[29] and visualized these parameters. The results of this study quantitatively demonstrated that either the β-value or A_{peak} was higher in m-HCC, while A_{120} tended to decrease as the grade of differentiation lessened. In the present study, either β-value or A_{peak} was smaller in p-HCC than in m-HCC. One reason for this might be derived from the technical issue in selecting ROI. As described in

Table 3 Parameter β of HCCs according to tumor differentiation

Histological differentiation	Homo β	Hetero β	Total
w-HCCs	19	0	19
m-HCCs	15	7	22
p-HCCs	0	8	8
Total	34	15	49

β-values in poorly differentiated HCC (p-HCC) samples had significantly larger variations in terms of time and space than in other HCCs ($P < 0.001$ for well-differentiated HCCs [w-HCCs]; $P < 0.01$ for moderately differentiated HCCs [m-HCCs]). Hetero β, the distribution of β value within the tumor is heterogeneous and/or irregular in time and space; Homo β, the distribution of β-value within the tumor is homogeneous and/or regular in time and space or shows almost the same pattern as that in the surrounding normal liver parenchyma.

Methods, above, we set ROI to cover the whole tumor. Because three of eight p-HCCs contained an avascular area inside the tumor indicating central necrosis, the data from p-HCC might include those avascular areas, which might affect the results of this study. In this way, although analysis of parameters can objectively evaluate the vascularity of the tumors, it may not be accurate if the ROI is not selected properly. To overcome this problem, we have developed a parametric imaging technique which visualizes parameters such as the β-value or A value.[30] Although parametric imaging itself is not quantitative, it can provide information of either β-value or A value relative to the adjacent normal liver parenchyma, and their localization in the tumor, by mapping these blood flow parameters within the tumor.

Table 4 Parameter A of HCCs according to tumor differentiation

Histological differentiation	Hyper A	Iso A	Hypo A	Total
w-HCCs	0	17	2	19
m-HCCs	0	4	18	22
p-HCCs	0	0	8	8
Total	0	21	28	49

The A value in well-differentiated HCCs (w-HCCs) were significantly higher than those in moderately differentiated HCC (m-HCC) and poorly differentiated HCC (p-HCC) ($P < 0.001$). Hyper A, A value that is higher than those in the adjacent non-tumor parenchyma; Hypo A, A value that is lower than those in the adjacent non-tumor parenchyma; Iso A, A value that is equal to the adjacent non-tumor parenchyma.

Consistent with the quantitative analysis of blood flow parameters, parametric imaging demonstrated that the β-value was significantly higher in m-HCC compared to the adjacent normal liver parenchyma, while it was almost the same between tumor and normal parenchyma in w-HCC, and thus the β-value was shown to be relatively higher in m-HCC than in w-HCC. The A_{120} was lower in p-HCC compared to the adjacent normal liver parenchyma, and thus was relatively lower in p-HCC compared to the other HCCs. On the other hand, w-HCC was spatially and temporally homogeneous and/or regular or showed almost the same pattern as that in the normal liver parenchyma in the β-value (Fig. 2a), while some m-HCCs and all p-HCCs were heterogeneous and/or irregularly color-coded with the β-value, either spatially or temporally (Fig. 4a). In this way, it was possible to evaluate not only either the β or A values relative to the adjacent normal liver parenchyma, but also their localization in the tumor, by mapping them within the tumor.

It is known that w-HCC histologically shows a normal portal structure, in which abnormal arteries, which do not run together with the bile duct, have not developed fully.[31] Therefore, either the β or A value in w-HCC would be similar to that in the adjacent normal liver parenchyma. This state may correspond to w-HCC. As the grade of differentiation advances, the abnormal arteries develop in the tumor together with the loss of normal portal structure. Either β-value or A_{peak} increases due to the development of abnormal arteries, while A_{120} decreases as the total vascular bed reduces due to the loss of normal portal structure.[31] This state may correspond to m-HCC. If the grade of differentiation advances further, circulation failure may develop due to either vascular invasion to feeding arteries or development of tumor embolism in the tumor vessels or efferent vessels, which leads to the irregular distribution of blood flow and reduction in both the β and A values. This state corresponds to p-HCC. There have been studies reporting that the angiogenesis of HCC is well correlated with the pathological process of differentiation,[32] as well as some angiogenesis factors being strongly expressed in w-HCC, while their expression reduces in m- or p-HCCs where angiogenesis is completed.[33] These pathophysiologies may lie in the background of the results of the present study.

There are, however, some limitations to the present study. We only included lesions with FNB that were complicated with HCC and thus we did not evaluate tumors other than HCC. The small number of p-HCC is another limitation of our study. On the other hand, there were sometimes cases with tumors located in a deeper region from the body surface, where no focal sign could be observed in all the phases, possibly because of the attenuation of ultrasound and especially at low MI harmonic imaging. Deep attenuation is one of the weak points of this method.

As for the safety of the contrast agent, no side-effects were observed in any patients in this study. Unlike the contrast agents used for CT imaging, SonoVue is non-iodine, and the injected volume is at most 5 mL, and therefore possible side-effects, such as an allergic reaction to iodine or renal or cardiac overload, are less likely to occur.

In conclusion, the vascular flow within HCC could be evaluated in detail, either by quantitative analysis of blood flow parameters or using parametric imaging. Quantitative analysis of blood flow parameters revealed that the β-value was the largest in moderately differentiated HCC, followed by poorly and well differentiated HCC in this order, while the A value was the largest in well differentiated HCC, followed by moderately and poorly differentiated HCC in this order. According to parametric imaging analysis, the β-values showed a more various distribution as HCC grades changed from well to poorly differentiated. Taken together, not only quantitative analysis of blood flow parameters, but also imaging analysis was considered important. The results of this study show the feasibility of non-invasive preoperative diagnosis of histological differentiation of HCC using CEUS with a certain accuracy and objectivity.

REFERENCES

1 Di Bisceglie AM. Hepatitis C and hepatocellular carcinoma. *Hepatology* 1997; 26 (3 Suppl 1): 34S–8S.
2 El-Serag HB, Mason AC. Rising incidence of hepatocellular carcinoma in the United States. *N Engl J Med* 1999; 340: 745–50.
3 Colombo M. Hepatocellular carcinoma. *J Hepatol* 1992; 15: 225–36.
4 Collier J, Sherman M. Screening for hepatocellular carcinoma. *Hepatology* 1998; 27: 273–8.
5 Trinchet JC, Beaugrand M. Treatment of hepatocellular carcinoma in patients with cirrhosis. *J Hepatol* 1997; 27: 756–65.
6 Bruix J. Treatment of hepatocellular carcinoma. *Hepatology* 1997; 25: 259–62.
7 Mor E, Kaspa RT, Sheiner P, Schwartz M. Treatment of hepatocellular carcinoma associated with cirrhosis in the era of liver transplantation. *Ann Intern Med* 1998; 129: 643–53.

8 Bruix J, Sherman M, Llovet JM *et al.* Clinical management of hepatocellular carcinoma: conclusions of the Barcelona-2000 EASL Conference. *J Hepatol* 2001; 35: 421–30.
9 Nicolau C, Catala V, Vilana R *et al.* Evaluation of hepatocellular carcinoma using SonoVue, a second generation ultrasound contrast agent: correlation with cellular differentiation. *Eur Radiol* 2004; 14: 1092–9.
10 Tanaka M, Nakashima O, Wada Y, Kage M, Kojiro M. Pathomorphological study of Kupffer cells in hepatocellular carcinoma and hyperplastic nodular lesions in the liver. *Hepatology* 1996; 24: 807–12.
11 Kanematsu M, Hoshi H, Takao H, Sugiyama Y. Abdominal wall tumor seeding at sonographically guided needle-core aspiration biopsy of hepatocellular carcinoma. *AJR* 1997; 169: 1198–9.
12 Takamori R, Wong LL, Dang C, Wong L. Needletract implantation from hepatocellular cancer: is needle biopsy of the liver always necessary? *Liver Transpl* 2000; 6: 67–72.
13 Torzilli G, Minagawa M, Takayama T *et al.* Accurate preoperative evaluation of liver mass lesions without fine-needle biopsy. *Hepatology* 1999; 30: 889–93.
14 Kim SH, Lim HK, Lee WJ, Cho JM, Jang HJ. Needle-tract implantation in hepatocellular carcinoma: frequency and CT findings after biopsy with a 19.5-gauge automated biopsy gun. *Abdom Imaging* 2000; 25: 246–50.
15 Amano S, Ebara M, Yajima T *et al.* Assessment of cancer cell differentiation in small hepatocellular carcinoma by computed tomography and magnetic resonance imaging. *J Gastroenterol Hepatol* 2003; 18: 273–9.
16 Ebara M, Fukuda H, Kojima Y *et al.* Small hepatocellular carcinoma: relationship of signal intensity to histopathologic findings and metal content of the tumor and surrounding hepatic parenchyma. *Radiology* 1999; 210: 81–8.
17 Numata K, Tanaka K, Kiba T *et al.* Contrast-enhanced, wide-band harmonic gray scale imaging of hepatocellular carcinoma. *J Ultrasound Med* 2001; 20: 89–98.
18 Wilson SR, Burns PN, Murdali D *et al.* Harmonic hepatic US with microbubbles contrast agents: initial experience showing improved characterization of hemangioma, hepatocellular carcinoma and metastasis. *Radiology* 2000; 215: 147–51.
19 Choi BI, Kim TK, Han JK, Kim AY, Chang KS, Park JP. Vascularity of hepatocellular carcinoma: assessment with contrast-enhanced second harmonic versus conventional power Doppler US. *Radiology* 2000; 214: 381–6.
20 Kim TK, Choi BI, Han JK, Hong HS, Park SH, Moon SG. Hepatic tumor: contrast agent-enhancement patterns with pulse-inversion harmonic US. *Radiology* 2001; 216: 411–17.
21 Tanaka S, Ioka T, Oshikawa O, Hamada Y, Yoshioka F. Dynamic sonography of hepatic tumors. *AJR* 2001; 177: 799–805.
22 International Working Party. Terminology of nodular hepatocellular lesions. *Hepatology* 1995; 22: 983–93.
23 Wei K, Jayaweera AR, Firoozan S *et al.* Quantification of myocardial blood flow with ultrasound-induced destruction of microbubbles administered as a constant venous infusion. *Circulation* 1998; 97: 473–83.
24 Hotta N, Tagava T, Maeno T *et al.* Advanced dynamic flow imaging with contrast-enhanced ultrasonography for the evaluation of tumor vascularity in liver tumors. *Clin Imaging* 2005; 29: 34–41.
25 Solbiati L, Tonillini M, Cova L, Goldberg N. The role of contrast-enhanced ultrasound in the detection of focal liver lesions. *Eur Radiol* 2001; 11 (Suppl 3): E15–26.
26 Nicolau C, Catala V, Vilana R *et al.* Evaluation of hepatocellular carcinoma using SonoVue, a second generation ultrasound contrast agent: correlation with cellular differentiation. *Eur Radiol* 2004; 14: 1092–9.
27 Fan Z-H, Chen M-H, Dai Y *et al.* Evaluation of primary malignancies of liver using contrast-enhanced sonography: correlation with pathology. *AJR* 2006; 186: 1512–19.
28 Ding H, Kudo M, Onda H *et al.* Hepatocellular carcinoma: depiction of tumor parenchymal flow with intermittent harmonic power Doppler US during the early arterial phase in dual-display mode. *Radiology* 2001; 220: 349–56.
29 Huang-Wei C, Bleuzen A, Olar M *et al.* Differential diagnosis of focal nodular hyperplasia with quantitative parametric analysis in contrast-enhanced sonography. *Invest Radiol* 2006; 41: 363–8.
30 Sugimoto K, Moriyasu F, Kamiyama N, Metoki R, Iijima H. Parametric imaging of contrast ultrasound for the evaluation of neovascularization in liver tumors. *Hepatol Res* 2007; 37: 464–72.
31 Ueda K, Terada T, Nakanuma Y *et al.* Vascular supply in adenomatous hyperplasia of the liver and hepatocellular carcinoma: a morphometric study. *Hum Pathol* 1992; 23: 619–26.
32 Miyaaki H, Fujimoto M, Kurogi M *et al.* Pathomorphological study on small nodular lesions in hepatitis C virus-related cirrhosis. *Oncol Rep* 2005; 14: 1469–74.
33 Hisai H, Kato J, Kobune M *et al.* Increased expression of angiogenin in hepatocellular carcinoma in correlation with tumor vascularity. *Clin Cancer Res* 2003; 9: 4852–9.

Hepatology Research 2008; 38: 790–799 doi: 10.1111/j.1872-034X.2008.00331.x

Original Article

Analysis of morphological vascular changes of hepatocellular carcinoma by microflow imaging using contrast-enhanced sonography

Katsutoshi Sugimoto,[1] Fuminori Moriyasu,[1] Naohisa Kamiyama,[2] Ryo Metoki,[1] Masahiko Yamada,[1] Yasuharu Imai[1] and Hiroko Iijima[3]

[1]*Department of Gastroenterology & Hepatology, Tokyo Medical University, 6-7-1 Nishishinjuku, Shinjuku-ku, Tokyo, 160-0023, Japan,* [2]*The Ultrasound Systems Development Department, Toshiba Medical Systems Corporation, 1385, Shimoishigami, Otawara-shi, Tochigi 324-8550, Japan, and* [3]*Department of Diagnostic Ultrasound, Medical Imaging Center, Hyogo College of Medicine, 1-1 Mukogawa-cho, Nishinomiya, Hyogo 663-8501, Japan*

Aim: To determine whether the findings of microflow imaging (MFI), composed of a flash replenishment and a maximum intensity holding sequence, using contrast-enhanced sonography, correlate with the degree of histological differentiation of hepatocellular carcinoma (HCC).

Methods: This study was approved by the institutional review board; patients gave informed consent. The samples comprised of 61 nodules histologically diagnosed as HCC: 20 well-differentiated, 26 moderately-differentiated, and 15 poorly-differentiated HCC. SonoVue was used as the ultrasound (US) contrast agent. The US equipment used was a SSA-770 A with the imaging mode set at MFI. MFI is an imaging method combining flash replenishment imaging and maximum intensity holding. Two independent readers (readers 1 and 2) classified the microflow images into four patterns: (i) normal pattern; (ii) cotton pattern; (iii) vascular pattern; and (iv) dead wood pattern. The results were compared with the degree of histopathological differentiation of the HCC.

Results: In each of the 61 HCC, blood vessels in the tumor were clearly resolved down to their fine branches. With regard to the relationship between imaging patterns and the histological findings, it was found (with high percentages) that the normal and cotton patterns were associated with well-differentiated HCC, that the vascular pattern was associated with moderately-differentiated HCC, and that the dead wood pattern was associated with poorly-differentiated HCC. If HCC with the normal and cotton patterns were assessed as well differentiated and those with the vascular or dead wood pattern were assessed as moderately or poorly differentiated, the sensitivity, specificity, and accuracy of these assessments were found to be 85%, 92.7%, and 90%, respectively, for reader 1, and 85%, 82.9%, and 83.6%, respectively, for reader 2.

Conclusion: The angioarchitecture and hemodynamics of HCC could be evaluated in detail using MFI. The results of this study demonstrate the feasibility of a non-invasive preoperative diagnosis of the histological differentiation of HCC using MFI.

Key words: contrast agent, hepatocellular carcinoma, histological differentiation, microflow imaging, ultrasonography

INTRODUCTION

HEPATOCELLULAR CARCINOMA (HCC) is the most common primary liver cancer, usually occurring as a complication of chronic liver disease and most often arising in a cirrhotic liver.[1–3] Therefore, the accurate surveillance of patients with liver cirrhosis is of great clinical importance because they are at increased risk of HCC.[4] The accurate and early diagnosis of HCC is essential for the treatment of affected patients. Surgical resection, liver transplantation, and percutaneous radiofrequency ablation (RFA) are potentially curative therapies for some patients.[5–8]

The ultrasound (US) findings of a focal liver lesion are often non-specific without contrast. Thus it is necessary to perform dynamic computed tomography (CT) or magnetic resonance imaging (MRI), or both for its characterization.[9–15] In addition to imaging studies, a fine needle biopsy (FNB) is recommended for all nodules with a diameter less than 2 cm, because in these cases it is difficult to distinguish HCC from other conditions using imaging techniques alone.[9]

It is known that more poorly-differentiated HCC are associated with a higher biological grade,[16] and thus determining the degree of differentiation is critical in clinical practice. Vascular invasion is one of the most important determinants of tumor grade and has also been reported to be correlated with the degree of differentiation.[17] It is therefore essential to conduct comprehensive imaging studies, as well as FNB, to diagnose the type and degree of differentiation of tumors. However, concerns have been raised about the risk of seeding during FNB aspiration of HCC in patients who will undergo liver transplantation or surgical resection,[11–18] which has been estimated to be up to 3.4%.[11] Diagnosing the degree of differentiation of HCC without biopsy has therefore been gaining more attention. In addition, while local therapies represented by RFA have recently been used widely, some authors have suggested that patients with poorly-differentiated HCC should be treated by primary surgery, because of the high incidence of local recurrence.[22] Diagnosing the degree of differentiation by imaging studies has therefore been suggested to be essential for determining the therapeutic application.

Recent advances in US technology, including harmonic imaging and the availability of US contrast agents, have improved the usefulness of US in the characterization of focal liver lesions, including HCC.[19–27] In particular, vascular imaging has been used to help determine the tissue type of focal liver lesions. Vascularity and/or morphological changes of the tumor vessels provide diagnostic information. For instance, a spoke wheel structure of the vessels is characteristic of focal nodular hyperplasia. In dynamic contrast US studies, we can observe the tumor vessels in the early arterial phase 10–30 s after an intravenous injection of contrast agent, at which time the tumor parenchyma is not yet opacified with the contrast agent.[24] Except for large-sized blood vessels, most of the vascular structure becomes blurred and obscured in the parenchymal opacification with contrast agents.[28] It is well known that microbubble contrast agents are destroyed by US exposure if the mechanical index (MI) of the transmitting pulse is higher than the microbubble destruction threshold. The flash replenishment sequence (FRS) consists of the destruction of microbubbles in the scan volume under exposure to a high MI US and visualization of reperfusion filled with fresh microbubbles under low MI harmonic imaging. This has been used for vascular imaging and quantitative analysis of myocardial perfusion[29] and hepatic parenchymal blood flow.[30] Microflow imaging (MFI; Toshiba Medical Systems, Otawara, Japan) was developed because the combination of FRS and the maximum intensity holding sequence was expected to make it possible to visualize vascular structure with high special resolution and vascular continuity. To our knowledge, this is the first study correlating the findings of MFI using SonoVue (Bracco, Milan, Italy), a second-generation US contrast agent, with the degree of cellular differentiation.

The aim of this study was to determine whether the MFI findings correlate with the degree of cellular differentiation.

METHODS

Study population

THE STUDY INCLUDED 61 patients with HCC ranging from 8 to 50 mm (mean ± SD, 21.5 ± 10.9 mm) that had been clearly visualized on conventional sonograms for the first time during the 18 months from July 2005 to December 2006. The patients included were 34 men and 27 women with an age range of 41–83 years (mean age, 70.7 ± 7.9 years). For patients with more than one focal lesion with a similar appearance at baseline gray-scale US, we selected the largest and most conspicuous lesion for this study. This study had the approval of the institutional ethics review board of Tokyo Medical University, Tokyo, Japan; all patients gave informed consent. Specimens from hepatic masses were obtained with a 20-gauge US-guided FNB. The degree of cellular differentiation (defined as well-, moderately-, or poorly-differentiated HCC) was determined according to the International Working Party classification.[31]

Sonologists

Three sonologists from our institution, who had 8 (KS), 20 (FM), and 15 (M.Y) years of experience in liver US imaging were involved in this study. Each sonologist had at least 5 years of experience in microbubble contrast, material-enhanced US of the liver, was aware of the patients' clinical histories, and was blinded to the biopsy results.

Sequence for MFI

A schematic illustration of MFI is shown in Figure 1. The FRS was performed manually by the operator. The maximum-hold processing started just after the burst

Correspondence: Dr Katsutoshi Sugimoto, *Department of Gastroenterology and Hepatology, Tokyo Medical University, 6-7-1 Nishishinjuku, Tokyo 160-0023, Japan. Email: sugimoto@comsat.ne*

Received 21 May 2007; revision 28 December 2007; accepted 3 January 2008.

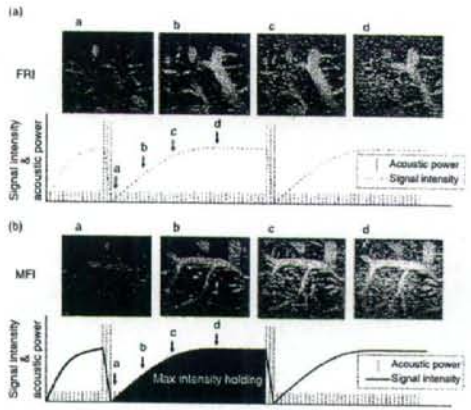

Figure 1 Scan sequences of (a) flash replenishment imaging (FRI) and (b) microflow imaging (MFI). Acquisition signals during replenishment after high mechanical index burst scanning are depicted with the maximum intensity holding technique in the MFI sequence. Each microbubble is recognized on the FRI images. However, continuous visualization of small blood vessels markedly improves on MFI images. (a) Acoustic power (|), Signal intensity (—); (b) Acoustic power (|), Signal intensity (—).

scan. The burst scan consisted of high MI (1.3–1.6) scanning of five frames. Low MI (0.07–0.09) scanning started again just after the high MI burst scanning to visualize fresh microbubble contrast agents flowing into the scanning volume.

The maximum intensity holding sequence was started simultaneously with flash replenishment low MI imaging, which maintained maximum brightness on each pixel and was displayed as a persistent vision. When the next burst scan was performed, max-hold processing was reset and this process was repeated several times to see the liver parenchyma and tumor tissue perfusion. The accumulation time for each MFI sequence was 10–15 s, depending on the perfusion of the target tissue.

Imaging techniques

SonoVue, the contrast agent used in this study, consists of sulfur hexafluoride microbubbles surrounded by phospholipids. The average diameter of a microbubble is 2.5 μm. SonoVue was injected as a 1.5 mL bolus into an antecubital vein using a 21-gauge peripheral intravenous cannula, followed by an injection of 10 mL saline solution at a rate of 1.0 mL/s. The US equipment used was a SSA-770 A (Aplio, Toshiba Medical Systems, Japan) with a 3.75 MHz convex transducer (PSK-375BT). The imaging mode was wideband harmonic imaging (commercially called pulse subtraction) with transmission and reception frequencies of 3.75 and 7.5 MHz, respectively. When a suspected lesion was identified, a dynamic contrast-enhanced ultrasonography (CEUS) was performed with the focus depth beyond the region of interest using the following settings: frame rate, 15 fps, and dynamic range, 35 dB. A low MI (0.07–0.09) was selected to avoid the disruption of microbubbles.

The region of interest was observed continuously for approximately 3 min from the time of injection. The arterial phase was timed for 45 s after the completion of the flash, after which we defined an extended portal venous phase, and this phase encompassed the commonly described interval from 45 to 70 s after injection, as well as the remainder of the observation period. Because the microbubbles of the contrast agent were purely intravascular, there was no interstitial or equilibrium phase. Enhancement in the extended portal venous phase showed progressive decay during approximately 3 min until the baseline appearance was observed again.[12]

We performed MFI once at the arterial phase and twice at the portal venous phase. Images and clips were stored on the hard disk for offline analysis. Among the three microflow (MF) images thus obtained, the MF image in which the vascular architecture was most clearly visualized was selected (KS) and kept for later analyses. Data obtained in dynamic studies other than MFI were excluded from the analyses.

Retrospective analysis

Digital cine clips stored on a PC were reviewed retrospectively on screen by two independent readers (RM and YI). Both were sonologists with 5 (RM) and 10 (YI) years of experience in using microbubble contrast agents. They were not involved in the US scanning. These readers were blinded to the identification, clinical histories, biopsy results, and other imaging findings of the patients. Cine clips were presented in random order, and any identifying information was masked. Prior to the reading, the readers were shown eight similar examples of MFI to establish a standardized approach to the interpretation of the information provided in the imaging sequences. The two readers were requested to classify each image as one of the following four patterns: normal, cotton, vascular, and dead wood patterns. In the normal pattern, the border between tumoral and non-tumoral regions was slightly indistinct, and the vascular architecture in the tumoral region was similar to that in the adjacent non-tumoral region (Fig. 2c). In the cotton pattern, the border between the tumoral and non-tumoral regions was distinct, but tumoral blood vessels were not clearly visualized and the tumor appeared pale as a whole, as if it was stained (Fig. 3c). In the vascular pattern, tortuous and meandering tumoral blood vessels were visualized clearly, and the tumor was imaged pronouncedly as a whole (Fig. 4c). In the dead wood pattern, tumoral blood vessels were visualized clearly, but they gradually tapered off and were interrupted suddenly (Fig. 5c). As a result, the distribution of the blood vessels was spatially heterogeneous in the tumor.

Statistical analyses

Statistical analyses were performed with a computer software package (StatMate III for Windows; Atoms, Tokyo, Japan). Baseline characteristics of the patients and HCC are expressed as mean ± SD. The relationship between the tumor size and pathological grading was analyzed with Fisher's exact test. A value of $P < 0.05$ was considered statistically significant. Sensitivity was defined as $TN/(TN + FN)$, specificity as $TN/(TP + FP)$, and overall accuracy as $(TP + TN)/(TP + TN + FP + FN)$, where TP is the number of true positive diagnoses, FN is the number of false negative diagnoses, TN is the number of true negative diagnoses, and FP is the number of false positive diagnoses.

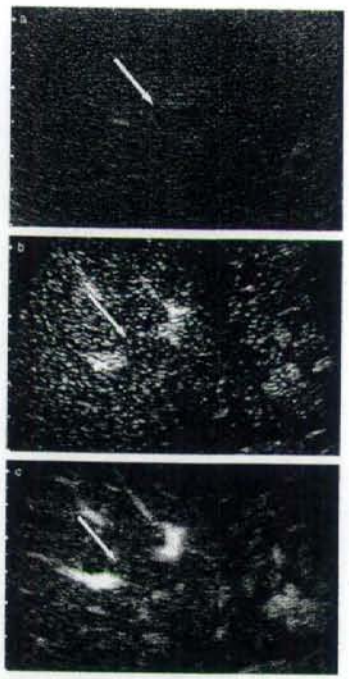

Figure 2 A 77-year-old woman with a 10-mm-diameter, well-differentiated hepatocellular carcinoma (HCC) in the right lobe of her liver. (a) Baseline ultrasound image show a focal hypoechoic HCC (arrow) in the right hepatic lobe. (b) Conventional harmonic image obtained during the portal venous phase—that is, 46 s after injection of the microbubble contrast agent—shows HCC (arrow) with an iso or slightly hypoechoic appearance relative to the adjacent liver. (c) Microflow image obtained during the portal venous phase—that is, 50 s after injection of the microbubble contrast agent—shows the blood vessel architecture more distinctly than the conventional harmonic image. Border between the tumoral and normal regions is not distinct. Blood vessel architecture in the tumoral region is almost identical with that in the adjacent normal hepatic parenchyma. Properties are characteristic of the normal pattern.

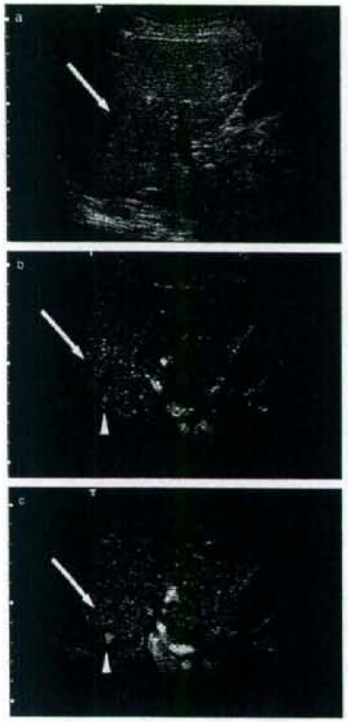

Figure 3 A 75-year-old man with a 28-mm-diameter, well-differentiated hepatocellular carcinoma (HCC) in the right lobe of his liver. (a) Baseline ultrasound image shows a HCC (arrow) with mosaic pattern appearance in the right hepatic lobe. (b) Conventional harmonic image obtained during the arterial phase—that is, 25 s after injection of the microbubble contrast agent—shows HCC (arrow) with a slightly hyperechoic appearance relative to the adjacent liver. Nodule-in-nodule appearance (arrow head) is demonstrated as a hypervascular spot in a slightly hypervascular nodule. (c) Microflow image obtained during the arterial phase—that is, 30 s after injection of the microbubble contrast agent—shows the blood vessel architecture more distinctly than the conventional harmonic image. Border between the tumoral and non-tumoral regions is distinct, but tumoral blood vessels are not clearly visible. Contrast-enhanced image of the tumoral region looks as if it was stained. Properties are characteristic of the cotton pattern. Nodule-in-nodule appearance (arrow head) is also more visible than in the conventional harmonic image.

RESULTS

Technical performance

A TOTAL OF 61 examinations were analyzed. All examinations were technically satisfactory for MFI.

Histological findings

The final diagnoses of the HCC were as follows: well-differentiated HCC in 20 cases (32.8%), ranging in diameter from 8 to 22 mm (mean ± SD, 15.3 ± 4.6 mm), moderately-differentiated HCC in 26 cases (42.6%), ranging in diameter from 10 to 40 mm (mean ± SD, 20.7 ± 8.5 mm), and poorly-differentiated HCC in 15 cases (24.6%), ranging in diameter from 15 to 50 mm (mean ± SD, 31.3 ± 13.8 mm). The results of tumor size and histopathology are shown in Table 1. The tumor size was significantly larger in poorly-differentiated HCC than in the other HCC ($P < 0.01$ for well-differentiated HCC, $P < 0.05$ for moderately differentiated HCC). In total, 100% (20/20) of well-differentiated HCC were smaller than 30 mm, 88.5% (23/26) of moderately-differentiated HCC were smaller than 30 mm, and 46.7% (7/15) of poorly-differentiated HCC were larger than 30 mm.

Blinded reading

The two independent readers classified the MF images into the four patterns, that is, normal, cotton, vascular, and dead wood. Their results were compared with the degree of histopathological differentiation of HCC. With both readers 1 (Table 2) and 2 (Table 3), there were trends for the normal and cotton patterns to be associated with well-differentiated HCC, the vascular pattern to be associated with moderately-differentiated HCC, and the dead wood pattern to be associated with poorly-differentiated HCC. In addition, neither reader found moderately- or poorly-differentiated HCC exhibiting the normal pattern or well-differentiated HCC exhibiting the dead wood pattern. If HCC with normal and cotton patterns were assessed to be well differentiated and those with vascular or dead wood patterns were assessed to be moderately or poorly differentiated, the sensitivity, specificity, and accuracy of such assessments were found to be 85%, 92.7% and 90%, respectively, for reader 1, and 85%, 82.9%, and 83.6%, respectively, for reader 2 (Table 4).

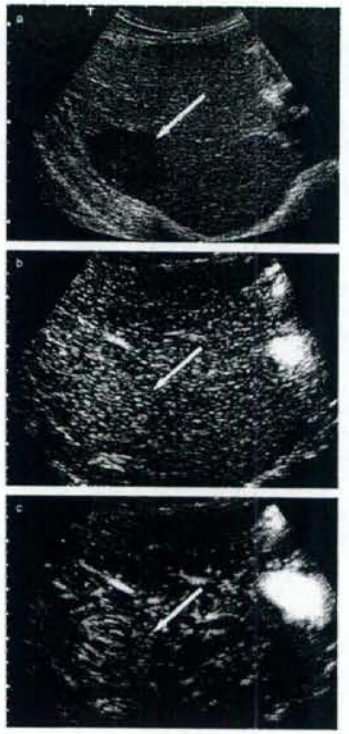

Figure 4 A 78-year-old man with a 30-mm-diameter, moderately-differentiated hepatocellular carcinoma (HCC) in the right lobe of his liver. (a) Baseline ultrasound image shows a focal hypoechoic HCC (arrow) in the right hepatic lobe. (b) Conventional harmonic image obtained during the portal venous phase—that is, 50 s after injection of the microbubble contrast agent—shows HCC (arrow) with homogeneous enhancement relative to the adjacent liver. (c) Microflow image obtained during the portal venous phase—that is, 55 s after injection of the microbubble contrast agent—shows the blood vessel architecture more distinctly than the conventional harmonic image. Border between the tumoral (arrow) and non-tumoral regions was distinct. Proliferation of tortuous and meandering blood vessels is clearly visible. Properties are characteristic of the vascular pattern.

DISCUSSION

THE DEVELOPMENT OF HCC is characterized by angiogenesis and the detection of new arterial vasculature in a focal liver lesion in a cirrhotic liver aids in the identification of HCC. HCC is a hypervascular tumor best diagnosed by spiral dynamic CT and dynamic MRI, because both techniques can evaluate the vascularity of the tumor using contrast enhancement.[9–15] Under dynamic CT or MRI, HCC typically presents a hypervascular pattern in the arterial phase and wash out in the late phase. However, the equipment required for such evaluations may not be available in small peripheral hospitals, and these procedures are usually more expensive than US. In addition, CT has the potential risk of radiation exposure.

Microbubble-based US contrast agents increase the intensity of the blood flow signal, improving the detection of flow in the hepatic artery and small vessels, and are as effective as CT contrast agents in assessing lesion perfusion.[21] Contrast-specific modes, such as advanced dynamic flow (ADF, Toshiba Medical Systems, Japan), associated with the contrast agent Levovist (Schering AG, Berlin, Germany), allow the evaluation of microvascularization of focal liver lesions, improving their characterization.[33] However, because Levovist's microbubbles are too sensitive to the US pulse, intermittent scanning (i.e. non-real-time imaging method) has to be used.[23] The new contrast agents, such as SonoVue, are more stable and resistant to US exposure and radiate sufficient harmonic signals by low MI transmission power, which allows continuous real-time imaging.[34] Also, from a clinical point of view, the real-time examination with SonoVue can acquire detailed information and time efficiency for the examination

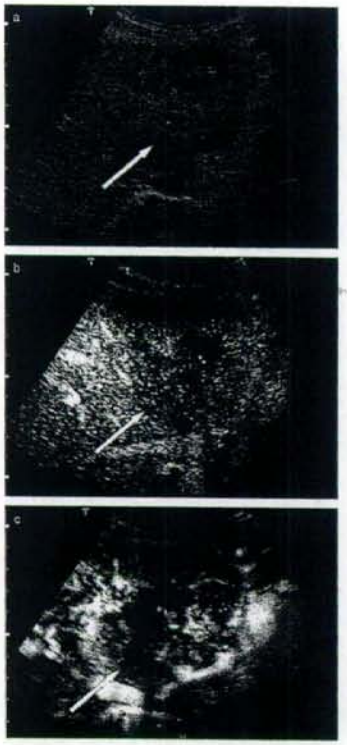

Figure 5 A 69-year-old woman with a 50-mm-diameter, poorly-differentiated hepatocellular carcinoma (HCC) in the left lobe of her liver. (a) Baseline ultrasound image shows a HCC (arrow) with mosaic pattern appearance in the left hepatic lobe. (b) Conventional harmonic image obtained during the portal venous phase—that is, 48 s after injection of the microbubble contrast agent—shows HCC (arrow) with heterogeneous enhancement. An avascular area, which is believed to be a necrotic region, is also noted in the tumor. (c) Microflow image obtained during the portal venous phase—that is, 53 s after injection of the microbubble contrast agent—shows tumoral blood vessels clearly. However, they are sparser than in moderately-differentiated HCC. Tapering and interruption of the vessels may be noted. Properties are characteristic of the dead wood pattern.

itself. It is suggested to be superior to Levovist in the evaluation of the hemodynamic status of focal liver lesions.

Several authors have reported on the behavior of the microbubbles in HCC.[23,24,26,27,34] Solbiati *et al.*[34] described a diffuse enhancement during the arterial phase that decreases during the portal venous and late phases, presenting a hypoechoic appearance in 54 of 61 HCC (88.5%), while in the remaining seven, they found a non-homogeneous enhancement related to necrotic changes. Nicolau *et al.*[33] reported that almost all HCC (96.2%) showed intratumoral enhancement in the arterial phase with a wash out in the late phase in 74 of 104 HCC (71.2%). Four HCC in their study without arterial enhancement in the CEUS were found to be well-differentiated HCC. They also found significant differences between the degree of cellular differentiation in the enhancement pattern of the HCC in the portal and late phases. Fan *et al.* also reported that moderately- to poorly-differentiated HCC had significantly shorter wash-out times compared to well-differentiated HCC, suggesting that CEUS is useful for determining the degree of differentiation of HCC[26].

In these studies, HCC was diagnosed on the basis of the degree of contrast enhancement of the tumor in the arterial phase and the degree of wash out in the portal and late phases. In the present study, we used MFI, a new imaging method developed by combining FRS and max intensity holding, and observed the fine architecture of blood vessels in the tumor and changes in their distribution, and thereby diagnosed HCC.

MF images could be classified into the following four patterns: normal, cotton, vascular, and dead wood patterns. Two readers classified each MF image into one of these four patterns, and the degree of histological differentiation of each lesion was compared with the pattern of its MF image. There were trends that the normal and cotton patterns were found in well-differentiated HCC, he vascular pattern was found in moderately-differentiated HCC, and the dead wood pattern was found in poorly-differentiated HCC. This result suggested the possibility that the degree of histopathological differentiation of HCC could be assessed with considerable accuracy using MFI.

According to a histological examination of HCC by Ueda *et al.*,[37] the portal region in nodules (including the normal portal vein and the hepatic artery) decreased in size, while increasing the malignancy of HCC, and became unobservable in moderately- and poorly-differentiated HCC. A few unpaired arteries, which took courses independent of the bile duct, that is, abnormal- or newly-growing arteries, were observed in atypical adenomatous hyperplasia. The unpaired arteries gradually increased in number with increasing malignancy of the tumor, and proliferated markedly in moderately-differentiated HCC.

It is conceivable therefore that even though the portal region partially decreases in size in well-differentiated HCC, this stage still has a recognizable portal region and only a few unpaired arteries. This stage seems to correspond to the normal and cotton patterns. According to Kojiro *et al.*,[38] small HCC less than approximately 2 cm in diameter may be grossly classified into two major types: a vaguely nodular type and a distinctly nodular type. They are markedly different from each other not only morphologically, but also biologically. In the present study, needle biopsies were used to obtain specimens for the histological examination. Differentiating tumors of the vaguely nodular type from those of the distinctly nodular type was consequently difficult. It seems to be possible, however, that the normal pattern

Table 1 Tumor size and histopathology of 61 lesions

Histological differentiation	Tumor size (mm)				
	<20	20–30	31–40	41–50	Total
Well-differentiated HCC	13	7	0	0	20
Moderately-differentiated HCC	13	10	3	0	26
Poorly-differentiated HCC	4	4	3	4	15
Total	30	21	6	4	61

Tumor size was significantly greater in poorly-differentiated hepatocellular carcinoma (HCC) than in other HCC. ($P < 0.01$ for well-differentiated HCC, $P < 0.05$ for moderately-differentiated HCC)

Table 2 MFI patterns of HCC according to histological differentiation (reader 1)

Histological differentiation	MFI patterns (reader 1)				Total
	Normal	Cotton	Vascular	Dead wood	
Well-differentiated HCC	8	9	3	0	20
Moderately-differentiated HCC	0	3	21	2	26
Poorly-differentiated HCC	0	0	3	12	15
Total	8	12	27	14	61

All data are actual values. HCC, hepatocellular carcinoma; MFI, microflow imaging.

Table 3 MFI patterns of HCC according to histological differentiation (reader 2)

Histological differentiation	MFI patterns (reader 2)				Total
	Normal	Cotton	Vascular	Dead wood	
Well-differentiated HCC	10	7	3	0	20
Moderately-differentiated HCC	0	6	18	2	26
Poorly-differentiated HCC	0	1	8	6	15
Total	10	14	29	8	61

All data are actual values. HCC, hepatocellular carcinoma; MFI, microflow imaging.

Table 4 Diagnostic performance of MFI at retrospective analysis

Performance parameter	MFI	
	Reader 1	Reader 2
Sensitivity	85.0 (17/20)	85.0 (17/20)
Specificity	92.7 (38/41)	82.9 (34/41)
Accuracy	90.2 (55/61)	83.6 (51/61)

Hepatocellular carcinoma with normal and cotton patterns were found to be well-differentiated and those with vascular or dead wood patterns were assessed to be moderately or poorly differentiated.
All data are percentages. Unless stated, numbers in parentheses are the numbers of lesions used to calculate the percentage. MFI, microflow imaging.

corresponded to the vaguely nodular type (early-stage HCC),[29] whereas the cotton pattern corresponded to the distinctly nodular type. The vascular pattern in the classification of MF images seems to reflect the next stage in malignancy, in which unpaired arteries have proliferated and the portal region has disappeared. With further progression of malignancy, feeding arteries are infiltrated by tumor cells located nearby or by cells in embolic tumors, and efferent vessels are blocked by tumoral emboli. As a result, circulatory disorders occur and blood flow in the tumor becomes spatially heterogeneous. The dead wood pattern seems to represent this stage. The histopathological changes described in this paragraph are considered to provide a background for the results of the present study.

The principal limitation of this study was that specimens for histopathological diagnosis of the degree of differentiation of HCC were obtained by FNB. The specimen obtained by FNB allows us to evaluate only a small part of the HCC lesion, which had been produced through a process called multistep hepatocarcinogenesis, that is, the successive development of the well-differentiated HCC from the dysplastic nodule through the dysplastic nodule with malignant foci, and consequently had histopathological heterogeneity inside. However, surgical verification is obtained infrequently, especially in patients with HCC, because small HCC lesions are often treated with transcatheter arterial chemoembolization or percutaneous ablation, especially in cirrhotic patients whose functional reserve is severely impaired.

A second limitation was that MFI has been clinically available to reconstruct the fine structure of the tumor vessels using the maximum intensity projection method. However, careful image acquisition is required when constructing MFI, that is, to avoid the blur due to the motion of both probe position and patient breathing. However, automatic motion correction devices are being developed to overcome this problem. Consequently, the problem of motion artifacts is expected to be resolved in the near future.

As for the safety of the contrast agent, no adverse reactions were observed in any patients in this study. Unlike the contrast agents used for CT imaging, SonoVue is non-iodine based and the injected volume is at most 5 mL. Therefore, possible adverse reactions, such as an allergic reaction to iodine or renal or cardiac overload, are less likely to occur.

In conclusion, the angioarchitecture and hemodynamics of HCC could be evaluated in detail using MFI. The results of this study show the feasibility of non-invasive preoperative diagnosis of histological differentiation of HCC using CEUS, with a high degree of accuracy and objectivity.

REFERENCES

1 Di Bisceglie AM. Hepatitis C and hepatocellular carcinoma. *Hepatology* 1997; 26: 34S–38S.
2 El-Serag HB, Mason AC. Rising incidence of hepatocellular carcinoma in the United States. *N Engl J Med* 1999; 340: 745–50.
3 Colombo M. Hepatocellular carcinoma. *J Hepatol* 1992; 15: 225–36.
4 Collier J, Sherman M. Screening for hepatocellular carcinoma. *Hepatology* 1998; 27: 273–8.
5 Trinchet JC, Beaugrand M. Treatment of hepatocellular carcinoma in patients with cirrhosis. *J Hepatol* 1997; 27: 756–65.
6 Bruix J. Treatment of hepatocellular carcinoma. *Hepatology* 1997; 25: 259–62.
7 Mor E, Kaspa RT, Sheiner P, Schwartz M. Treatment of hepatocellular carcinoma associated with cirrhosis in the era of liver transplantation. *Ann Intern Med* 1998; 129: 643–53.
8 Bruix J, Sherman M, Llovet JM *et al.* Clinical management of hepatocellular carcinoma: conclusions of the Barcelona 2000 EASL Conference. *J Hepatol* 2001; 35: 421–30.
9 Takayasu K, Moriyama N, Muramatsu Y *et al.* The diagnosis of small hepatocellular carcinomas: efficacy of various imaging procedures in 100 patients. *AJR* 1990; 155: 49–54.
10 Srklarak J, Silverman PM, Charnsangavej C. Imaging in the diagnosis, staging, treatment, and surveillance of hepatocellular carcinoma. *AJR* 2003; 180: 441–54.
11 Lee HM, Lu DS, Krasny RM, Busuttil R, Kadell B, Lucas J. Hepatic lesion characterization in cirrhosis: significance of arterial hypervascularity on dual-phase helical CT. *AJR* 1997; 169: 125–30.

12 Teefey A, Hildeboldt CC, Dehdashti F *et al.* Detection of primary hepatic malignancy in liver transplant candidates: prospective comparison of CT, MR imaging, US, and PET. *Radiology* 2003; 226: 533–42.
13 Baron RL, Oliver JH III, Dodd GD III, Nalesnik M, Holbert BL, Carr B. Hepatocellular carcinoma: evaluation with biphasic, contrast-enhanced, helical CT. *Radiology* 1996; 199: 505–11.
14 Miller WJ, Baron RL, Dodd GD 3rd, Federle MP. Malignancies in patients with cirrhosis: CT sensitivity and specificity in 200 consecutive transplant patients. *Radiology* 1994; 193: 645–50.
15 Brancatelli G, Baron RL, Peterson MS, Marsh W. Helical CT screening for hepatocellular carcinoma in patients with cirrhosis: frequency and causes of false-positive interpretation. *AJR* 2003; 180: 1007–14.
16 Kojiro M. Histopathology of liver cancers. *Best Pract Res Clin Gastroenterol* 2005; 19: 39–62.
17 Sun B, Zhang S, Zhang D *et al.* Vasculogenic mimicry is associated with high tumor grade, invasion and metastasis, and short survival in patients with hepatocellular carcinoma. *Oncol Rep* 2006; 16: 693–8.
18 Kanematsu M, Hoshi H, Takao H, Sugiyama Y. Abdominal wall tumor seeding at sonographically guided needle-core aspiration biopsy of hepatocellular carcinoma. *AJR* 1997; 169: 1198–9.
19 Takamori R, Wong LL, Dang C, Wong L. Needletract implantation from hepatocellular cancer: is needle biopsy of the liver always necessary? *Liver Transpl* 2000; 6: 67–72.
20 Torzilli G, Minagawa M, Takayama T *et al.* Accurate preoperative evaluation of liver mass lesions without fine-needle biopsy. *Hepatology* 1999; 30: 889–93.
21 Kim SH, Lim HK, Lee WJ, Cho JM, Jang HJ. Needle-tract implantation in hepatocellular carcinoma: frequency and CT findings after biopsy with a 19.5-gauge automated biopsy gun. *Abdom Imaging* 2000; 25: 246–50.
22 Yu HC, Cheng IS, Lai KH *et al.* Factors for early tumor recurrence of single small hepatocellular carcinoma after percutaneous radiofrequency ablation therapy. *World J Gastroenterol* 2005; 11: 1439–44.
23 Numata K, Tanaka K, Kiba T *et al.* Contrast-enhanced, wide-band harmonic gray scale imaging of hepatocellular carcinoma. *J Ultrasound Med* 2001; 20: 89–98.
24 Wilson SR, Burns PN, Muradali D *et al.* Harmonic hepatic US with microbubbles contrast agents: initial experience showing improved characterization of hemangioma, hepatocellular carcinoma and metastasis. *Radiology* 2000; 215: 147–51.
25 Choi BI, Kim TK, Han JK, Kim AY, Chang KS, Park JP. Vascularity of hepatocellular carcinoma: assessment with contrast-enhanced second harmonic versus conventional power Doppler US. *Radiology* 2000; 214: 381–6.
26 Kim TK, Choi BI, Han JK, Hong HS, Park SH, Moon SG. Hepatic tumor: contrast agent-enhancement patterns with pulse-inversion harmonic US. *Radiology* 2001; 218: 411–17.
27 Tanaka S, Ioka T, Oshikawa O, Hamada Y, Yoshioka F. Dynamic sonography of hepatic tumors. *AJR* 2001; 177: 799–805.
28 Sirlin CB, Girard MS, Baker KG, Steinbach GC, Deiranieh LH, Mattrey RF. Effect of acquisition rate on liver and portal vein enhancement with microbubble contrast. *Ultrasound Med Biol* 1999; 25: 331–8.
29 Wei K, Jayaweera AR, Firoozan S *et al.* Quantification of myocardial blood flow with ultrasound-induced destruction of microbubbles administrated as a contrast venous infusion. *Circulation* 1998; 97: 473–83.
30 Metoki R, Moriyasu F, Kamiyama N *et al.* Quantification of hepatic parenchymal blood flow by contrast ultrasonography with flash-replenishment imaging. *Ultrasound Med Biol* 2006; 32: 1459–66.
31 International Working Party. Terminology of nodular hepatocellular lesions. *Hepatology* 1995; 22: 983–93.
32 Burns PN, Wilson SR. Focal liver masses: enhancement patterns on concoidance of US scans with CT scans and MR images. *Radiology* 2007; 242: 162–74.
33 Hotta N, Tagawa T, Maeno T *et al.* Advanced dynamic flow imaging with contrast-enhanced ultrasonography for the evaluation of tumor vascularity in liver tumors. *Clin Imaging* 2005; 29: 34–41.
34 Solbiati L, Tonillini M, Cova L, Goldberg N. The role of contrast-enhanced ultrasound in the detection of focal liver lesions. *Eur Radiol* 2001; 11: E15–26.
35 Nicolau C, Catala V, Vilana R *et al.* Evaluation of hepatocellular carcinoma using SonoVue, a second generation ultrasound contrast agent: correlation with cellular differentiation. *Eur Radiol* 2004; 14: 1092–9.
36 Zhi-Hui Fan, Min-HuaChen Ying Dai et al. Evaluation of primary malignancies of liver using contrast-enhanced sonography: correlation with pathology. *AJR* 2006; 186: 1512–19.
37 Ueda K, Terada T, Nakanuma Y *et al.* Vascular supply in adenomatous hyperplasia of the liver and hepatocellular carcinoma: a morphologic study. *Hum Pathol* 1992; 23: 619–26.
38 Kojiro M, Nakashima O. Histopathologic evaluation of hepatocellular carcinoma with a special reference to small early stage tumor. *Semin Liver Dis* 1999; 19: 267–76.
39 Liver Cancer Study Group of Japan. *General Rules for the Clinical and Pathological Study of Primary Liver Cancer*, 2nd edn. Tokyo: Kanehara, 2003.

Intervirology

Intervirology 2008;51(suppl 1):17–26
DOI: 10.1159/000122595

Published online: June 10, 2008

Diagnostic Accuracy of Imaging for Liver Cirrhosis Compared to Histologically Proven Liver Cirrhosis

A Multicenter Collaborative Study

Masatoshi Kudo[a] Rong Qin Zheng[b] Soo Ryang Kim[g] Yoshihiro Okabe[c] Yukio Osaki[c] Hiroko Iijima[e] Toshinao Itani[f] Hiroshi Kasugai[d] Masayuki Kanematsu[i] Katsuyoshi Ito[j] Norio Usuki[h] Kazuhide Shimamatsu[k] Masayoshi Kage[k] Masamichi Kojiro[k]

[a]Department of Gastroenterology and Hepatology, Kinki University School of Medicine, Osaka-Sayama, Japan; [b]Department of Ultrasound, Third Affiliated Hospital, Sun Yat-Sen University, Guangzhou, China; Departments of Gastroenterology, [c]Osaka Red Cross Hospital and [d]Osaka Center for Cancer and Cardiovascular Disease, Osaka, [e]Division of Hepatobiliary and Pancreatic Diseases, Department of Medicine, Hyogo Medical College, Nishinomiya, Departments of Gastroenterology, [f]Nishi-Kobe Medical Center and [g]Kobe Asahi Hospital, and [h]Department of Radiology, Kobe City West Hospital, Kobe, [i]Department of Radiology, Gifu University School of Medicine, Gifu, [j]Department of Diagnostic Radiology, Kawasaki Medical School, Kurashiki, and [k]Department of Pathology, Kurume University School of Medicine, Kurume, Japan

Key Words

CT · Diagnostic accuracy · Diagnostic imaging · Imaging modalities · Liver cirrhosis · MRI · Multicenter study · Ultrasonography · Receiver-operating characteristic analysis

Abstract

Objective: To evaluate the diagnostic accuracy of liver cirrhosis by imaging modalities, including CT, MRI and US, compared to results obtained from histopathological diagnoses of resected specimens. ***Materials and Methods:*** CT, MRI and US examinations of 142 patients with chronic liver disease who underwent surgery for complicated hepatocellular carcinoma (<3 cm in diameter) in 10 institutions were blindly reviewed in a multicenter study by three radiologists experienced in CT, MRI and US. The images were evaluated for five imaging parameters (irregular or nodular liver surface, blunt liver edge, liver parenchymal abnormalities, liver morphological changes and manifestations of portal hypertension) using a severity scale. The diagnostic imaging impression score was also calculated. Patients were histologically classified into chronic hepatitis (CH; n = 54), liver cirrhosis (LC; n = 71) and pre-cirrhosis (P-LC; n = 17) by three pathologists, independently, who reviewed the resected liver specimens. The results of the three imaging methods were compared to those from histological diagnoses, and a multivariate analysis (stepwise forward logistic regression analysis) was performed to identify independent predictive signs of cirrhosis. The diagnostic efficacies for LC and early cirrhosis were also compared among CT, MRI and US using a receiver-operating characteristic (ROC) curve analysis. ***Results:*** The differences in the five imaging parameters evaluated by CT, MRI and US between LC and CH were statistically significant ($p < 0.001$)

KARGER

Fax +41 61 306 12 34
E-Mail karger@karger.ch
www.karger.com

0300–5526/08/0517–0017$24.50/0

Accessible online at:
www.karger.com/int

Masatoshi Kudo, MD, PhD
Department of Gastroenterology and Hepatology
Kinki University School of Medicine, 377-2, Ohno-Higashi
Osaka-Sayama 589-8511 (Japan)
Tel. +81 723 66 0221, ext. 3149, Fax +81 723 67 2880, E-Mail m-kudo@med.kindai.ac.jp

except for the manifestations of portal hypertension on US. Irregular or nodular surface, blunt edge or morphological changes in the liver were selected as the best predictive signs for cirrhosis on US whereas liver parenchymal abnormalities, manifestations of portal hypertension and morphological changes in the liver were the best predictive signs on MRI and CT by multivariate analysis. The predictive diagnostic accuracy, sensitivity and specificity in discriminating LC from CH based on the best predictive signs were 71.9, 77.1 and 67.6% by CT; 67.9, 67.5 and 68.3% by MRI, and 66.0, 38.4 (lower than CT and MRI, $p = 0.001$) and 88.8% (higher than CT and MRI, $p = 0.001$) by US. According to the imaging impression scoring system, diagnostic accuracy, sensitivity and specificity were 67.0, 84.3 and 52.9% by CT; 70.3, 86.7 and 53.9% by MRI, and 64.0, 52.4 (lower than CT and MRI, $p = 0.0001$) and 73.5% (higher than CT and MRI, $p < 0.003$) by US. ROC analysis showed that MRI and CT were slightly superior to US in the diagnosis of LC but no statistically significant difference was found between them. For the pathological diagnosis of P-LC, cirrhosis was diagnosed in 59.5, 46.7 and 41.7% of the P-LC cases by US, CT and MRI, respectively, with no significant difference among these methods. ***Conclusion:*** US, CT and MRI had different independent predictive signs for the diagnosis of LC. MRI and CT were slightly superior to US in predicting cirrhosis, especially regarding sensitivity. Noninvasive imaging techniques play an important role in the diagnosis of cirrhosis, especially in the evaluation of P-LC.

Introduction

Liver cirrhosis (LC), which is defined as a diffuse process of architectural disorganization histologically characterized by fibrosis and regenerative nodules [1], has a tendency to progress to portal hypertension, hepatocellular dysfunction and hepatocellular carcinoma (HCC). In addition, progression from compensated to decompensated cirrhosis finally results in life-threatening complications such as liver failure or massive gastrointestinal hemorrhage [2, 3]. In the management of liver diseases, an accurate diagnosis is a prerequisite for effective treatment since proper medical treatments such as interferon therapy may slow disease progression.

Although laparoscopy-guided liver biopsy has been the standard method for the diagnosis of LC, it is invasive and not practical for the subsequent follow-up of patients. Furthermore, it is well known that even biopsy diagnosis fails to correctly differentiate between chronic hepatitis (CH) and LC. Biochemical and imaging examinations have been commonly used for the noninvasive clinical diagnosis of LC. The need for liver biopsy is reduced, if either or both of these approaches provide a correct diagnosis of LC, which is the main purpose of current investigations. Imaging modalities including ultrasonography (US), computed tomography (CT) and magnetic resonance imaging (MRI) play important roles in the clinical diagnosis of chronic liver diseases, the follow-up of the disease course and progression of the disease, as well as the detection of potential complications, e.g. HCC [4–7]. These methods seem especially crucial in patients with compensated LC and normal biochemical values showing no active inflammation.

The imaging characteristics of LC have been well described in previous studies [5–15]. The roles of different imaging modalities in the diagnosis of LC have also been discussed separately [8–13, 15–18] or as combinations of two imaging methods [14, 19, 20]. However, only a few studies reported the diagnosis of compensated LC [17, 21]. To the best of our knowledge, studies comparing different imaging techniques (CT, US and MRI) with macroscopically and histopathologically diagnosed LC and pre-cirrhosis (P-LC) have not been published yet.

The aim of this retrospective multicenter study was to evaluate the accuracy of three imaging modalities in the diagnosis of LC and P-LC, and to identify independent predictive imaging signs of cirrhosis by multivariate analysis.

Patients and Methods

Study Design

This study is a cross-over multicenter retrospective trial involving 10 Japanese hospitals and university centers. The study protocol was proposed by the Research Group of Diagnosis and Treatment of Liver Cirrhosis (Japanese Society of Gastroenterology) and approved by the institutional review boards of each center.

Patients

Information from 157 cases of HCC who underwent surgical treatment for tumor resection was collected within a 3-year period from 1997 to 2000 as part of a multicenter study, and only 142 cases were included in this study. Inclusion criteria were as follows: (a) histological manifestations of diffuse liver disease except for HCC and a clinical history of chronic liver disease based on persistent abnormalities in liver function tests, and (b) the main tumor nodule being <3 cm in diameter (lesions <3 cm negligibly affect liver morphology, hemodynamics and function).

There were a total of 104 men and 38 women, aged between 42 and 82 years (mean age, 64 years), with chronic liver disease

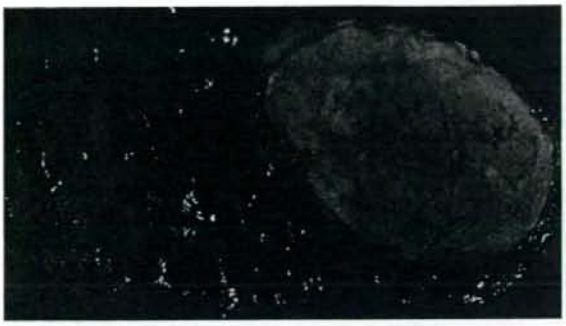

Fig. 1. Resected specimen showing HCC and background liver disease.

caused by hepatitis B viral infection (n = 23), hepatitis C viral infection (n = 97), alcohol damage (n = 2), other causes (n = 2) and unclear causes (n = 16). Clinical staging of cirrhosis was performed according to the Child-Pugh classification (grades A–C) based on a scoring system using variables for ascites, encephalopathy, bilirubin, albumin values and prothrombin time [22, 23].

Pathological Diagnosis

The resected liver specimens were used for histological diagnosis. The areas where there was no tumor lesion within the specimens were evaluated (fig. 1) macroscopically and microscopically with hematoxylin and eosin (HE), and Masson and Azan stains by three pathologists (K.S., M.K. and M.K.) in the Department of Pathology, Kurume University, independently and blindly without knowledge of clinical data except for the presence of liver tumors. The final diagnosis was determined when consensus was reached by at least two pathologists for each patient's specimen. In this study, there was no situation where all three pathologists disagreed on the same patient. Liver fibrosis stages were assessed according to the criteria of the international classification for the histological assessment of CH [24], in which fibrosis was classified from F_0 to F_3 with varying degrees of fibrosis (fig. 2a), and cirrhosis developed from CH was expressed as F_4 (fig. 2b). Namely, F_0 represented no fibrosis; F_1 was characterized by fibrous portal expansion; F_2 showed bridging fibrosis (portal-portal or portal-central linkage); F_3 was bridging fibrosis with lobular distortion (disorganization), and F_4 meant cirrhosis. Some cases of F_3 with progressing lobular architecture distortion and a tendency to form regenerative nodules but with no complete fibrotic septa and no obvious regenerative nodules in the liver were defined as P-LC (fig. 2c), and were excluded from both groups of LC and CH when making pathological diagnosis.

Imaging Interpretation

Imaging examinations including US, CT and MRI were retrospectively reviewed and scored independently in a random order by three blinded readers who were unaware of the patients' pathological and clinical data apart from HCC. Namely, three radiologists (N.U., M.K. and K.I.) specialized in liver imaging reviewed both CT and MRI scans, and three ultrasound experts

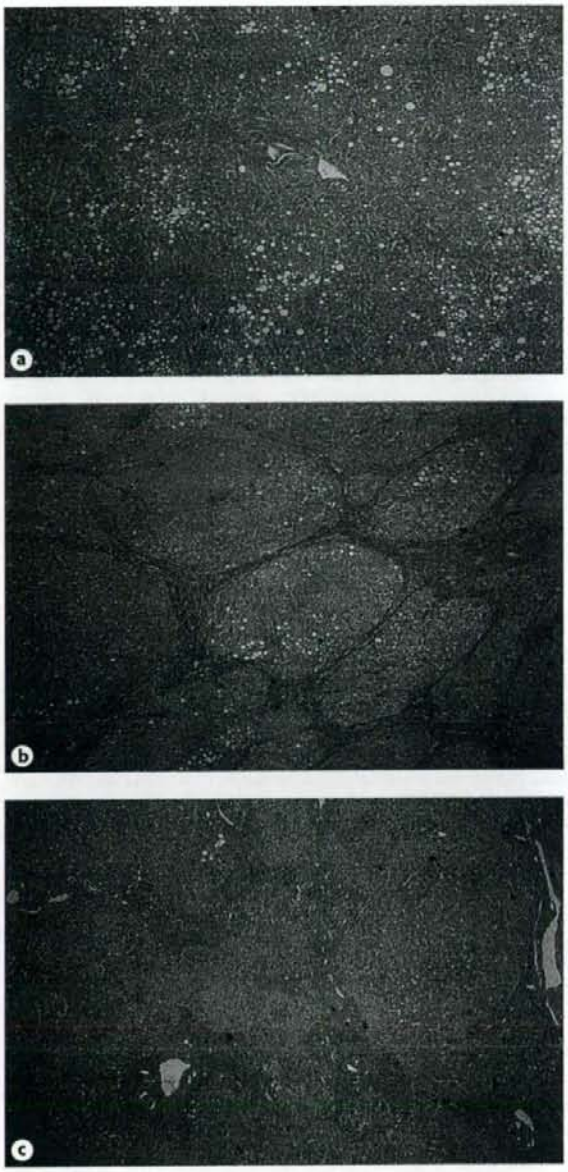

Fig. 2. Histopathological specimens showing mild fibrosis (F_1; **a**), regenerative nodular formation, suggesting LC (F_4; **b**) and findings of P-LC (**c**).

(T.I., Y.O. and H.I.) evaluated US data. All imaging examinations were performed according to routine clinical protocols within 2 weeks before the patients underwent surgery.

The imaging data were evaluated for the following five parameters: presence or absence of irregular or nodular liver surface, blunt liver edge, liver parenchymal abnormalities (coarseness, heterogeneity and regenerative nodules), liver morphological changes (including subitems of atrophy of the right lobe and the medial segment, hypertrophy of the lateral segment and the caudate lobe, widened pericholecystic space and enlargement in the periportal space), manifestations of portal hypertension (including subitems of splenomegaly, dilatation of the splenic vein, ascites and collaterals which presented at gastroesophageal and paraesophageal, paraumbilical, splenorenal shunt and other locations such as retroperitoneal and perisplenic mesenteric collaterals). The assessment of irregular and nodular surfaces, blunt edges, parenchymal abnormalities, splenomegaly, splenic vein dilatation, ascites and each subitem of liver morphological changes, i.e. atrophy of the right lobe and left medial segments, hypertrophy of the left lateral segment and caudate lobe, except for the enlargement of the pericholecystic space and periportal vein space (which were recorded as no = 0, yes = 1), was performed using a severity scale (none = 0, subtle = 1, definite = 2). Each subitem of the manifestations of portal hypertension was also scored (no = 0, yes = 1). With regard to the parameters of liver morphological changes and manifestations of portal hypertension, if one of the abovementioned subitems of these two parameters was positive (namely had a score of 1 or 2), then liver morphological changes or manifestations of portal hypertension existed and the scores of all the subitems were summed to give a combined score made of these two parameters.

Collateral circulation at gastroesophageal and paraesophageal, paraumbilical, splenorenal and other locations was not fully evaluated by US because most patients were examined to evaluate liver tumors, and US pictures were not taken to show the collaterals.

Imaging diagnostic impressions for each method were also independently made by the three blinded observers mentioned above based on a 5-point grading scale (definitive LC = 5, probable LC = 4, undetermined = 3, probably not LC = 2, definitively not LC = 1) according to the unified impression for the whole imaging manifestations.

Analysis of Items and Statistical Analysis

The methods of analysis of the items and statistics were as follows. (a) Univariate analysis was used to compare the various imaging findings between CH and LC using the Mann-Whitney U test. $p < 0.05$ was considered statistically significant. (b) Multivariate analysis was applied to assess independent effects of imaging parameters predicting the diagnosis of LC using a stepwise forward logistic regression analysis. (c) The χ^2 test was used to compare the efficacy of the three imaging methods (including diagnostic accuracy, sensitivity and specificity) in the diagnosis of LC based on significant predictive variables of imaging findings and imaging diagnostic impression scores. (d) The receiver-operating characteristic (ROC) analysis was applied to compare the diagnostic impression scores among the three imaging methods. The ROC curve was expressed with sensitivity plotted against specificity. The discrimination capacity was revealed by the location of the ROC curve (it was better that the curve was located more upward and left, and far from the chance line). The areas under the ROC curve were expressed as A_z. The diagnostic value was defined as low ($A_z = 0.50–0.70$), moderate ($A_z = 0.70–0.90$) and high ($A_z = 0.90–1.0$) [25]. (e) The χ^2 test was also performed to calculate and compare the frequency of possible cirrhosis in P-LC cases using the three imaging modalities.

Only cases in whom all imaging data of US, CT and MRI were available were included in the multivariate analysis and the comparison of diagnostic efficacies among the three imaging methods.

All patients had three records of each imaging finding score and imaging diagnostic impression score. When it was difficult to determine a score, the corresponding record was considered as a missing value and was not counted in the later statistical analysis.

For the assessment of interobserver variability of categorical imaging findings, a κ analysis was performed. The levels of agreement were defined as: no agreement ($\kappa < 0$), poor agreement ($\kappa = 0–0.4$), fair agreement ($\kappa = 0.41–0.60$), good agreement ($\kappa = 0.61–0.80$) and excellent agreement ($\kappa = 0.81–1.00$) [15].

Results

Pathological and Imaging Diagnosis

The pathological diagnostic results of the 142 cases were: CH in 54 cases, LC in 71 cases and P-LC in 17 cases (these cases did not take part in the statistical analysis for the diagnosis of LC). The results of the histological assessment of fibrosis stages were as follows: F_0 in 3 cases, F_1 in 8 cases, F_2 in 24 cases, F_3 in 36 cases and F_4 in 71 cases. In the 71 cases of LC, the Child-Pugh grade classification was: grade A in 65 cases (91.5%), grade B and grade C in 1 patient (1.4%) and undetermined grade in 4 cases (5.6%) because of missing laboratory data.

CT, MRI and US data were available for 132, 89 and 124 cases, respectively. Seventy-two cases (CH in 28 cases and LC in 34 cases) underwent all three imaging examinations before operation.

With regard to the interobserver variability in categorical imaging findings, κ values demonstrated fair agreement in CT and MRI (0.52 and 0.59, respectively), being poor in US (0.39).

Distinction between LC and CH

Univariate Analysis

The differences in the five imaging parameters (i.e. irregular and nodular liver surface, blunt liver edge, liver parenchymal abnormalities, liver morphological changes and manifestations of portal hypertension) evaluated by CT, MRI and US were statistically significant between LC and CH ($p < 0.001$) except for the manifestations of portal hypertension on US. Comparing the subitems of liver

Table 1. Comparison of imaging finding categories between LC and CH using different imaging modalities

Imaging finding parameters	CT			MRI			US		
	f	Z	p	f	Z	p	f	Z	p
Irregular and nodular surface	350	−9.037	0.000	231	−6.276	0.000	329	−6.078	0.000
Blunt edge	350	−6.511	0.000	231	−3.998	0.000	300	−5.522	0.000
Parenchymal abnormalities	351	−4.629	0.000	231	−6.008	0.000	328	−6.527	0.000
Morphological changes	351	−6.450	0.000	231	−5.517	0.000	327	−6.177	0.000
Atrophy of the right lobe	351	−3.913	0.000	231	−6.511	0.000	303	−5.046	0.000
Atrophy of the medial segment	347	−5.239	0.000	231	−3.248	0.001	168	−4.021	0.000
Hypertrophy of the lateral segment	347	−4.534	0.000	231	−5.760	0.000	281	−3.640	0.000
Hypertrophy of the caudate lobe	347	−3.350	0.001	231	−2.418	0.016	198	−4.153	0.000
Widened pericholecystic space	346	−4.453	0.000	231	−3.934	0.000	206	−2.563	0.000
Enlarged periportal space	348	−3.414	0.001	231	−2.467	0.014	20	−1.780	NS
Manifestations of portal hypertension	351	−7.990	0.000	231	−5.634	0.000	317	−0.315	NS
Splenomegaly	345	−7.585	0.000	231	−5.351	0.000	212	−2.019	0.044
Splenic vein dilatation	346	−5.757	0.000	231	−4.114	0.000	115	−1.627	NS
Ascites	351	−1.223	NS	231	−1.698	NS	313	−0.784	NS
Gastro- and esophageal varices	346	−2.783	0.005	231	−2.363	0.011			
Paraumbilical collaterals	346	−4.137	0.000	231	−3.344	0.001			
Splenorenal shunt	347	−2.733	0.006	230	−0.370	NS			
Other sites of collaterals	350	−2.901	0.004	231	−1.389	NS			

f = Frequency for which the imaging scores were available; Z = statistical value of the non-parametric test; NS = nonsignificant.

morphological changes and manifestations of portal hypertension, the imaging manifestations of ascites on CT, MRI and US indicated no significant difference between LC and CH. Furthermore, collaterals at splenorenal and other locations on MRI, and enlargement of the periportal space and dilatation of the splenic vein on US also showed no significant differences whereas the differences in other subitems of liver morphological changes and portal hypertension were statistically significant between LC and CH ($p < 0.05$; table 1; fig. 3).

Multivariate Analysis

The results of the stepwise forward logistic regression analysis with the pathological diagnosis of LC and CH as dependent variables and the five imaging parameters as independent variables are shown in table 2. Irregular and nodular liver surface, blunt liver edge and liver morphological changes were selected as the best predictive signs (significant independent variables) on US whereas liver parenchymal abnormalities, manifestations of portal hypertension and liver morphological changes were the best predictive signs on MRI; the results of CT were similar to those of MRI with one more variable (irregular and nodular liver surface). The predictive diagnostic accuracy, sensitivity and specificity that discriminated LC from CH based on the best predictive signs were 71.9, 77.1 and 67.6% by CT, respectively; 67.9, 67.5 and 68.3% by MRI, respectively, and 66.0, 38.4 (lower than CT and MRI, $p = 0.001$) and 88.8% (higher than CT and MRI , $p = 0.001$) by US (table 3), respectively.

Diagnostic Impression

According to the diagnostic imaging impression scores, LC corresponded to a score ≥4, and CH corresponded to a score <4. The diagnostic accuracy, sensitivity and specificity values were 67.0, 84.3 and 52.9% by CT; 70.3, 86.7 and 53.9% by MRI, and 64.0, 52.4 (lower than CT and MRI, $p = 0.0001$) and 73.5% (higher than CT and MRI, $p \leq 0.003$) by US, respectively (table 3).

ROC Analysis

The ROC curves of the three imaging modalities in the diagnosis of LC are shown in figure 4. MRI and CT were slightly superior to US with moderate A_z values of 0.788, 0.770 and 0.716, respectively, but no significant difference was found among these modalities.

Evaluation of P-LC

For the pathological diagnosis of P-LC as early cirrhosis, the imaging materials in cases of early cirrhosis avail-

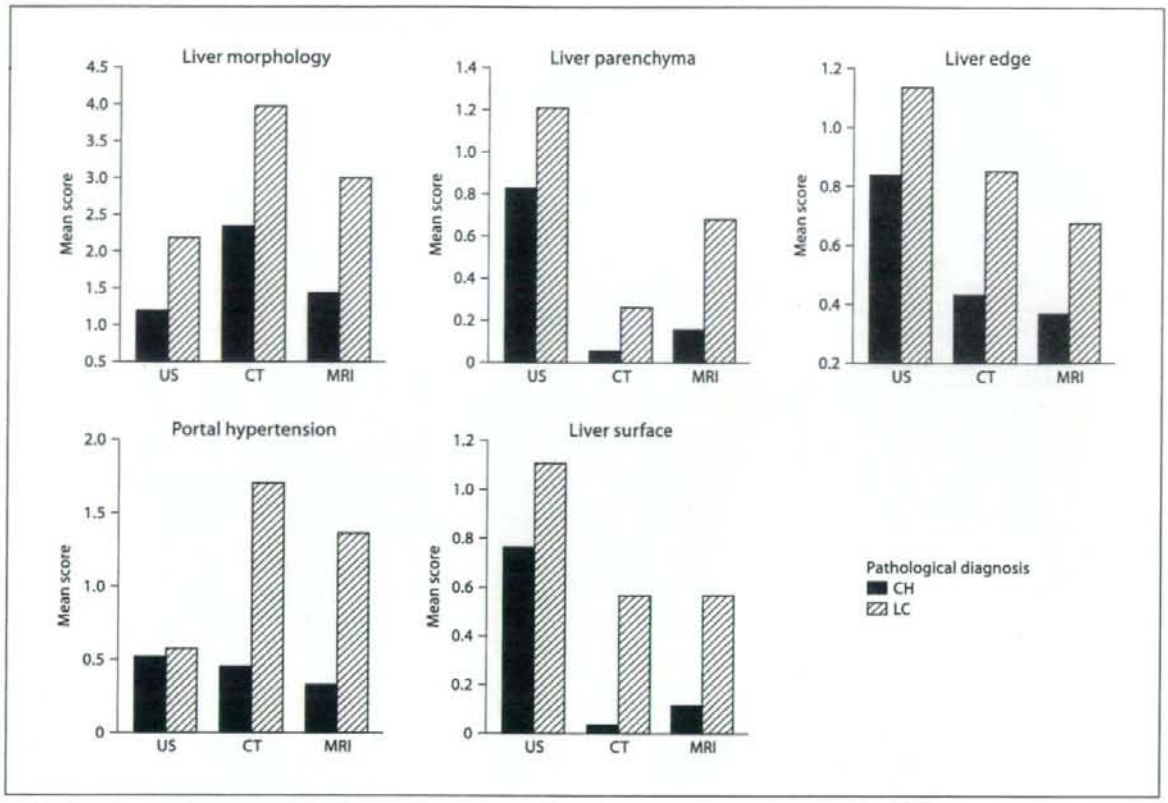

Fig. 3. Differences in the five imaging finding categories on US, CT and MRI compared to pathological diagnosis between LC and CH.

Table 2. Results of logistic regression: imaging finding categories versus pathological diagnosis for LC and CH

Selected independent variables	B	Odds ratio (95% confidence intervals)	p value
US			
Irregular and nodular surface	1.039	2.827 (1.123–7.118)	0.027
Blunt edge	0.985	2.677 (1.004–7.138)	0.049
Morphological changes	0.292	1.333 (0.996–1.799)	0.053
MRI			
Parenchymal abnormalities	1.003	2.726 (1.469–5.060)	0.001
Manifestations of portal hypertension	0.486	1.626 (1.119–2.363)	0.011
Morphological changes	0.280	1.323 (1.094–1.599)	0.004
CT			
Irregular and nodular surface	1.979	7.238 (2.572–20.369)	0.000
Parenchymal abnormalities	1.331	3.786 (1.288–11.129)	0.016
Manifestations of portal hypertension	0.321	1.379 (1.050–1.811)	0.021
Morphological changes	0.212	1.236 (1.043–1.465)	0.015

Table 3. Diagnostic accuracy, sensitivity and specificity of LC by different imaging modalities based on selected independent variables and imaging impression scores

	By selected independent variables, %			By imaging impression scores, %		
	accuracy	sensitivity	specificity	accuracy	sensitivity	specificity
US	66.0	38.4[a]	88.8[a]	64.0	52.4[b]	73.5[c]
CT	71.9	77.1	67.6	67.0	84.3	52.9
MRI	67.9	67.5	68.3	70.3	86.7	53.9

[a] $p = 0.001$; [b] $p = 0.0001$; [c] $p = 0.003$, vs. CT and MRI.

able in CT, US and MRI were 15, 14 and 12, respectively. The frequencies of imaging impression scores ≥4, which suggested cirrhosis by CT, US and MRI, were 46.7 (21/45, representing the scoring records), 59.5 (25/42) and 41.7% (15/36), respectively. There was no statistically significant difference in the frequencies of the three methods.

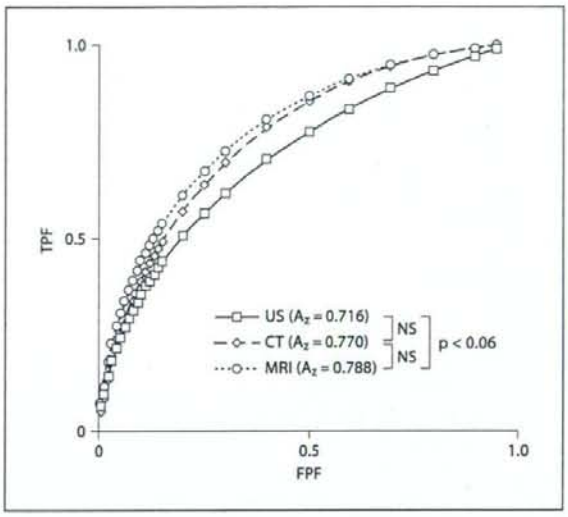

Fig. 4. ROC analysis shows no statistical difference between MRI, CT and US in the differentiation of LC from CH.

Discussion

Cross-sectional imaging is important in the detection of intra- and extrahepatic features of LC [5–7]. Alterations in liver morphology such as atrophy of the right lobe and left medial segment, hypertrophy of the left lateral segment and caudate lobe, enlargement of the pericholecystic and periportal spaces, nodular liver surface, abnormal hepatic texture at US and inhomogeneous attenuation at CT or inhomogeneous signal intensity at MRI have been documented as an indication of regenerative nodules. Furthermore, blunt liver edge, collateral circulation, splenomegaly and ascites were described as important imaging findings of LC in previous studies [4–21, 26–30].

In this study, we used three methods to evaluate imaging parameters, and integrated the results into five categories which were compared between LC and CH. The results showed that there were significant differences in the presence of irregular or nodular liver surface, blunt liver edge, liver parenchymal abnormalities and liver morphological changes among these imaging modalities. With respect to ascites, there was no significant difference because most of the patients included in this study had compensated LC and were suitable candidates for surgery. Significant differences existed for portal hypertension with CT and MRI, but not with US. One of the possible reasons for this difference was that the evaluation of the collaterals was rarely available by US due to the retrospective design of this study. In addition, the results showed that significant differences existed in all sites of collaterals on CT, but only in two sites on MRI. This might be explained by the fact that gradient echo sequences of MRI, which were considered more sensitive than spin echo sequences in detecting collateral circulation [5, 16], were not routinely used in this retrospective study.

In multivariate analysis, liver morphological change was one of the best predictive signs in all the three imaging methods while liver parenchymal abnormalities and manifestations of portal hypertension were the best predictive signs for both CT and MRI; the presence of an irregular or nodular liver surface was one of the best predictive signs of LC for both CT and US. These results suggest that the assessment of liver morphological changes and manifestations of portal hypertension by imaging, which is an advantage of cross-sectional imaging tech-

niques, is important for the diagnosis of LC. The results also indicated that MRI and CT were superior to US in the detection of parenchymal abnormalities and manifestations of portal hypertension. In previous studies, parenchymal nodules surrounded by reticulated low intensity network of fibrosis, i.e. direct features of LC, were better visualized by MRI than US or CT [31, 32]. CT is more sensitive than arterial portography for depicting a patent paraumbilical vein [33] and is efficient for determining shunt patency in cases inaccessible by sonography [31].

The diagnostic accuracy rates of the three imaging modalities based on both diagnostic impression scores, which was the simple way of estimating cirrhosis, and significant independent predictive signs were relatively low, especially in US, compared to previous reports [8–10, 13, 18, 27]. Furthermore, the diagnostic sensitivity of US was lower, but specificity was higher than for CT and MRI in the same patient groups. Differences in these results may be attributable, firstly, to the fact that most of our patients who could tolerate surgical treatments for the resection of complicated HCC had CH and compensated liver disease (91% cases were graded as Child A), namely, disease severity was relatively mild; therefore, the cirrhotic features of these cases were not so striking by imaging. Secondly, the majority of the patients included in this study underwent US to check for liver tumors, and an insufficient number of pictures of every section of the liver was stored for later retrospective reviews. Because real-time scanning and monitor-depending diagnosis are important in ultrasonography, diagnosis based on stored ultrasonographic pictures was relatively difficult. Thirdly, poor interobserver agreement of US due to subjectivity and the above-mentioned reasons might result in a decreased diagnostic accuracy because there was a correlation between diagnostic accuracy and interobserver agreement in a previous study [34]. Finally, the intercenter variability derived from the different techniques applied might also affect the diagnostic accuracy of US.

In spite of its relative low accuracy, US is still considered the method of choice for the examination of suspected hepatobiliary diseases, and it is valuable in the follow-up of patients with LC because of its low costs, easy performance, high patient compliance and its high sensitivity in the detection of small nodular lesions [35, 36].

Although percutaneous liver biopsy is considered as the conventional and important method for the diagnosis of LC and assessment of disease severity of chronic liver diseases, it has some limitations in addition to its invasiveness. The first one is the sampling error. It is well known that liver parenchymal damage in LC and CH is not uniform, i.e. there is a discordance of 50% on repeated liver biopsy specimens [37] and 24% of false-negative results in a series of blind liver biopsies [38]. Furthermore, the specimen size may influence the accuracy of the pathological diagnosis [39], and inadequate fragmented biopsy samples may fail to ensure proper evaluation [40]. In addition, in cases of macronodular cirrhosis, which is common in viral-induced cirrhosis, needle biopsy specimens may not suffice to sample the entire parenchymal nodules or fibrous septum, which are key components in establishing the diagnosis of cirrhosis. As a result, even advanced LC may result in nonspecific fibrotic changes and may not be correctly diagnosed as LC [6]. This situation may sometimes be encountered even in laparoscopic-guided biopsy.

In our study, resected liver specimens, which should be the gold standard for LC diagnosis, were used to assess pathological changes and make the diagnosis of LC when sample size was large enough and the sample error was reduced to a minimum, therefore providing much superior information than needle biopsy.

Interestingly, regarding P-LC, although histological diagnosis did not accurately match the LC criteria, approximately 50% of P-LC cases were diagnosed as LC by imaging. According to the criteria of the international classification of CH [24], cases with progressing lobular architecture distortion and a tendency to form regenerative nodules but with no complete fibrotic septa and no definite regenerative nodules were classified as F_3 although from a clinical point of view, the damage in liver hemodynamics and the incidence of liver cancer in these cases were similar to those of cirrhosis [41], which is regarded as P-LC (or early cirrhosis). In nearly half of our P-LC cases, LC was diagnosed using the imaging modalities, indicating that the imaging techniques could be important supplementary methods for the evaluation of early cirrhosis. Imaging allows the detection of the gross morphological features of cirrhosis and assessment of the intra- and extrahepatic vasculature; in some cases, imaging was able to establish a diagnosis of cirrhosis even though the histological diagnosis could not be ascertained [6, 17], which is one of the important roles of imaging diagnosis. However, the diagnostic accuracy and sensitivity of imaging techniques in the evaluation of early cirrhosis have to be confirmed in future studies.

There are several limitations of this study. Firstly, due to the retrospective design of the study, imaging interpretation criteria could not be standardized in detail, so interobserver variability was relatively high especially in